Possible experiments with very high energy cosmic neutrinos: the Dumand project

V. S. Berezinskiĭ and G. T. Zatsepin

Institute of Nuclear Studies, USSR Academy of Sciences
Usp. Fiz. Nauk **122**, 3–36 (May 1977)

PACS numbers: 13.15.+g, 12.30.Ez, 94.40.Te

CONTENTS

1. INTRODUCTION

Neutrinos with energies in excess of 10 TeV[1)] continue to remain the monopoly of nature. While specialists labor on designs of accelerators with energies of 10 TeV, gigantic natural accelerators produce somewhere in the depths of galaxies, and to a purpose unknown to us, particles with energies in excess of 10^{20} eV. Interactions of these particles with interstellar and intergalactic matter, and collisions in our own atmosphere, result in the creation of neutrinos with very high energies.

There is twofold interest in these cosmic neutrinos.

Firstly, they can be used to investigate interactions between neutrinos and matter at energies well in excess of the capabilities of accelerators planned for the future, i.e., between 10^{13} and 10^{15}–10^{16} eV.

Secondly, to use V. L. Ginzburg's phrase, high-energy metagalactic neutrinos present a new communication channel with the rest of the universe. The value of this channel is that, of all high-energy particles, it is only the neutrinos that are capable of traversing the universe. Thus, we have the possibility of recording in our time the neutrinos that were born in a distant cosmological epoch, say, ten billion years ago, in the course of turbulent astrophysical processes accompanied by bursts of high-energy cosmic rays.

The neutrino–nucleon interaction at 10–100 TeV can be studied in the flux of neutrinos produced in the earth's atmosphere by primary cosmic rays. The spectrum of the atmospheric neutrinos can be calculated quite reliably.

This is not an entirely new problem. Experiments on atmospheric neutrinos at energies between 10 and 100 GeV have been carried out with underground installations.[1] The most important conclusion, i.e., that the neutrino–nucleon cross section increases linearly with energy up to about 10–100 GeV,[3] was subsequently confirmed by accelerator experiments. Numerical results agree to within statistical error: the underground experiments yielded $\sigma=(0.55\pm0.2)\times10^{-38}E$, whereas accelerator experiments gave $\sigma=(0.83\pm0.11)\times10^{-38}E$ (in these expressions, σ is in cm^2 and E in GeV).

Because of the substantially lower flux of atmospheric neutrinos, transition to 10–100 TeV requires experiments on a different scale but, nevertheless, one can realistically expect that they will be performed in the near future.

At energies in excess of 10^{14} eV, the flux of atmospheric neutrinos is too low for detection by currently available methods. However, at these energies, and especially above 3×10^{15} eV, substantial fluxes of extragalactic neutrinos are expected to be present. Experiments with the latter neutrinos will pursue two aims.

Firstly, they will form the basis for neutrino astronomy (observation of distant cosmological epochs). High neutrino fluxes should be produced during the formation of galaxies and early star-forming processes. The frequent supernova explosions during this epoch lead to the creation of high-energy cosmic rays. The neutrinos are created during the collision of high-energy protons with the nuclei of interstellar and intergalactic gas, and with photons. The possibility of neutrino generation in the galaxy and in the intergalactic space by cosmic rays was noted as far back as 1963 by Ginzburg and Syrovatskiĭ,[4] who pointed out that underground neutrino experiments could yield important astronomical information. The important channel for the production of high-energy neutrinos is provided by collisions with remnant photons: $p+\gamma_{\text{rem}}\to n+\pi^+$, $\pi^+\to\mu^++\nu_\mu$, and $\mu^+\to e^++\nu_e+\tilde{\nu}_\mu$. The problem for neutrino astronomy is completely specified because the density of the target (remnant photons) is known for all cosmological epochs, the pion photoproduction cross section has been measured, and so the required quantity (flux of high-energy protons) is uniquely related to the measured quantity, i.e., the neutrino flux. Moreover, the low-energy edge

1) 1 TeV = 10^{12} eV.

of the neutrino spectrum determines the red shift of the epoch at which the cosmic-ray generation burst took place.

The second aim of neutrino experiments at $E \gtrsim 10^{14}$ eV is to investigate the interactions of neutrinos with nucleons and electrons. At first sight, it would appear that the absence of precise predictions of the neutrino flux will prevent measurement of neutrino cross sections. We shall show, however, that it is, in fact, possible to calibrate the apparatus against the neutrino flux. An important experiment with cosmic neutrinos at energies of 10^{15}–10^{16} eV may be the search for the W boson in the resonance reaction $\bar{\nu}_e + e^- \to W^- \to$ hadrons.

The possibility of deep underwater detection of neutrinos with the aid of Čerenkov radiation was discussed by A. E. Chudakov in 1969. A specific proposal for a cosmic neutrino experiment was put forward in the USA by a group of American universities and the Accelerator Center at Batavia.[5] One of the leading initiators of this project is F. Reines. The project is designated DUMAND, which is an abbreviation for Deep Underwater Muon And Neutrino Detection. The atmospheric neutrino experiment is called ATHENE (ATmosphere High-Energy Neutrino Experiment) and that with the extragalactic neutrinos is called UNICORN (UNderwater Interstellar COsmic Ray Neutrinos).[2)]

The DUMAND installation should take the form of a lattice of detectors (photomultipliers in transparent water-permeable spheres). The planned volume of the lattice is 10^9 m^3 (1 km × 1 km × 1 km). The installation will be located at a depth of 5 km in the ocean and will be shielded by this thickness of water from all particles other than neutrinos and high-energy ($E > 3$ TeV) muons. The photomultipliers at the lattice sites should record electromagnetic radiation emitted by electrons produced as a result of interactions of neutrinos and muons with particles in the aqueous medium. Čerenkov radiation due to muons in seawater has been recorded in the experiment reported in[2].

Deep underwater investigations are of major interest to oceanologists. So far, however, the influence has been in the other direction: oceanological studies of parameters such as the nature of the ocean floor, flow parameters near the floor, transparency of the water, and emission of radiation by microorganic systems have an important influence on the choice of location for the installation and its parameters. The most suitable location for the experiment is agreed to be the ocean-floor valley near the Hawaiian Islands.

The assembly of the system at a depth of 5 km gives rise to considerable technological difficulties, but the last conference showed that these problems could be solved by existing means.

Development work is being carried out on detectors, including the interesting spherical photomultiplier project.

The program of physics experiments involved in the DUMAND project has been published in a preliminary form in the proceedings of a recent conference.[5] In this paper, we shall base our account mainly on the detailed calculations performed in the USSR.

At the last conference on the DUMAND project, Askar'yan and Dolgoshein, and also Bowen, suggested an acoustic method for the detection of very high-energy neutrinos in the ocean. Preliminary experimental data are already in existence. They were obtained in accelerator experiments and indirectly confirm the possibility of this method. Acoustic detection should allow a substantial increase in the volume of the installation.

2. DUMAND: POSSIBILITIES OF DETECTION

In the DUMAND experiments, the detector is the water of the ocean itself, which responds with a flash of light to a collision of high-energy particle. This flash is produced as follows.

An incident particle colliding with a nucleus, or a nucleon that is part of it, transfers a considerable part of its energy to secondary particles which, in turn, produce a nuclear-electromagnetic shower as a result of further collisions with nuclei. When the shower reaches its maximum development, a large fraction of the electrons has energies lower than the so-called critical energy (73 MeV for water) at which ionization energy losses experienced by these electrons are comparable with radiative losses. As the electrons move through water, they produce optical Čerenkov radiation. Each electron emits photons at angle $\theta_C \approx 41°$ to its direction of motion and, since most of the electrons move in the direction of the shower axis, the Čerenkov photons are emitted mainly along the surface of a cone with angle $\theta_C \approx 41°$ relative to the shower axis. This radiation will be recorded by a set of photomultipliers arranged in a space lattice. The photomultiplier signal amplitude can be used to determine the shower energy and the signal arrival time the coordinates of the event. Since the radiation is emitted at a particular angle, the disposition of the responding detectors will define the direction of the shower axis, i.e., the direction of arrival of the primary particle. On the other hand, the highly directional character of the emission is the main difficulty in its detection. The point is that the radiation propagates in the form of a thin layer along the surface of a cone, and there is a large probability that it will miss the nearest detectors. At large distances, on the other hand, at which the thickness of the conical layer becomes greater, the light flux is highly attenuated by absorption in water.

A. Detection of showers and the magnitude of the detector lattice constant

Let us consider, very approximately, the magnitude of the lattice constant d for a cubic lattice formed by the detectors.

The angular distribution of the emitted Čerenkov photons relative to the shower axis, due to the angular distribution of the electrons, is shown in Fig. 1. These

[2)]This designation seems to us to be narrower than the scope of the actual planned experiment. We propose a different name: EXTHENE (EXTraterrestrial High-Energy Neutrino Experiment).

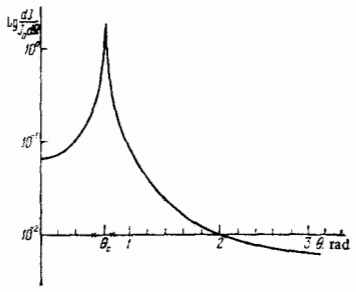

FIG. 1. Angular distribution of Čerenkov radiation from an electromagnetic-nuclear shower.[6] $dJ/d\Omega$ is the flux of photons per unit solid angle, J_0 is the total flux, and θ is the angle to the shower axis. The crosses on the horizontal axis indicate the angular interval within which half the energy is radiated ($\Delta\theta_{eff} = 0.2$); $\theta_c \approx 41°$ corresponds to the maximum flux.

calculations were carried out by Belyaev, Ivanenko, and Makarov.[6] It is clear from the figure that half the total radiated energy is localized within an angle $\Delta\theta_{eff} \approx 0.2$ rad relative to the cone surface. This produces a broadening of the conical light layer at large distances. The other reason for the broadening, which is important at short distances, is the finite length of the cascade.[7] Figure 2 illustrates the propagation of Čerenkov radiation away from the shower. At a distance l from the shower maximum, the illuminated area and volume are, respectively, given by

$$S = 2\pi l^2 \sin\theta_C \left(\Delta\theta_{eff} + \frac{2h}{l}\sin\theta_C\right), \quad (1)$$

and

$$V = \frac{2\pi}{3} l^3 \sin\theta_C \left(\Delta\theta_{eff} + \frac{3}{2}\frac{h}{l}\sin\theta_C\right), \quad (2)$$

where h is the length of the radiating part of the shower, $h \approx 3\sqrt{\ln E_H/\varepsilon}$ in t-units, E_H is the total energy of the shower, and the t-unit for water is 36 cm.

A relativistic electron emits about 200 Čerenkov photons in the optical region ($4\times10^{-5} - 7\times10^{-5}$ cm) per centimeter of path, and loses about 2 MeV by ionization at the same time. It follows that a total shower energy of 1 MeV corresponds to the emission of 100 Čerenkov photons. The flux of photons (number per unit area) at a distance l from the shower is given by

$$n_\gamma = \frac{100 E_0(\text{MeV})}{S} e^{-l/l_0}. \quad (3)$$

where l_0 is the absorption length in water and S is given by (1). We shall assume henceforth that $l_0 \approx 20$ m. This value was obtained as a result of measurements in pure ocean water at moderate depths,[5] but experts note that the transparency at a depth of 5 km in the region of the Hawaiian Islands may be greater by a factor of 1.5. The minimum flux of Čerenkov photons that is necessary for quantitative measurements will be assumed to be $n_\gamma \approx 0.6$ photon/cm^2, which corresponds to the incidence of 100 photons on a multiplier with photocathode diameter of about 15 cm and the release of 20 photoelectrons. When only the fact of detection need be recorded (for example, the passage of a muon), the release of 3–5 photoelectrons is sufficient, and the minimum detectable flux is then reduced to $n_\gamma \approx 0.09$ photon/cm^2. It was reported at the DUMAND-76 workshop that the US industry produced photomultipliers of hemispherical shape with a photo-cathode area of 300 cm^2. The minimum detectable flux (simple detection only) for these devices is then only $n_\gamma \approx 0.05$ photon/cm^2.

If we substitute $E_0 = 10^{13}$ eV and $n_\gamma \approx 0.6$ photon/cm^2 in (1)–(3), we obtain $h \approx 3.7$ m, $l \approx 68$ m, and $V \approx 1.1 \times 10^5$ m^3. Consequently, to produce a "good" signal in 10 detectors, the separation between them must be $d \approx 20$ m. It is clear from (1) and (2) that the parameter that determines the relative contribution of the finite length of the shower to the broadening of the light layer is

$$\eta = \frac{h\sin\theta_C}{l\,\Delta\theta_{eff}}.$$

In our example, $\eta = 0.18$, i.e., the broadening of the layer of light is dominated by the angular distribution of the Čerenkov radiation. As the distance l increases (the energy E_0 or the transparency of water increases), this effect becomes greater still and the shower may be approximated by a luminous point. At small distances l, the situation is dominated by the spatial broadening of the layer of light, due to the finite width of the shower.

In addition to the radiation emitted in the form of the ray cone (Fig. 1), there is also the anisotropic radiation component which occupies a large solid angle. It is due to the radiation emitted by electrons traveling at large angles to the shower axis. We shall show that this component illuminates at least all the detectors in the lattice cell in which the event has taken place.

About 1.5% of all the Čerenkov photons is emitted at 90° to the shower axis into a unit solid angle. We shall take this as the minimum isotropic intensity in the forward hemisphere. When $E_H = 10^{13}$ eV, the total number of "isotropic" photons in the forward hemisphere is $N_\gamma \sim 10^8$, and the flux at the distance $r = (\sqrt{3}/2)d$ is $n_\gamma = 2N_\gamma/3\pi d^2 \approx 5$ photon/cm^2.

The total number of detectors that have responded in the near zone is determined by the distance $r \sim 2l_0 - 2.5l_0$ from the shower and depends on the geometry of the installation. The most convenient arrangement is the tetrahedral lattice. Since the angular distribution of the radiation is highly inhomogeneous, the pulse heights produced by the detectors, and the distances between the responding detectors and the shower axis, are subject to strong fluctuations.

A typical event (for $E_H \sim 10^{13}$ eV) should appear as follows.

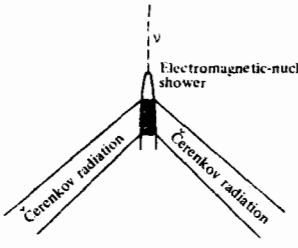

FIG. 2. Schematic representation of the emission of Čerenkov radiation by a shower.

About 10 detectors respond in the ray-cone layer. Most of these detectors lie at the end of the conical layer (at a distance of about 70 m), where the illuminated volume is at a maximum and the photon flux is close to the threshold value. The pulse heights generated by most detectors in the far zone will therefore reach the threshold value independently of the shower energy. The pulse heights from detectors intersected by the conical layer at shorter distances will be a measure of the energy, but this situation will be relatively rare. The geometric disposition of the detectors responding in the conical layer can be used to determine the direction of the shower axis. The pulse heights due to detectors in the near zone are very sensitive to the shower energy. However, the direction of the shower axis must be known before this energy is determined because the detector output depends on which particular part of the nonisotropic light flux the detectors have intercepted. In the near zone (angle $\theta > 1$ rad), the dependence of $(1/J_0)\,dJ/d\Omega$ on θ is weaker than in the far zone (Fig. 1). For example, when the angle is varied by $\Delta\theta \approx 50$ mrad, the quantity $(1/J_0)\,dJ/d\Omega$ changes by only 5–8%. The lattice cell in which the events take place is determined by the illuminated front wall of the detectors. The exact geometric coordinates of the shower can be found from the time distribution of pulses produced by different detectors.

The above estimates of the lattice constant d are almost trivial: it is physically clear that this quantity cannot greatly exceed the length l_0 necessary for the absorption of light in water. However, if the direction of the shower axis is determined in some other way (for example, with the aid of the muon in the reaction $\nu_\mu + N \to \mu^- + \text{hadrons}$), and the photomultiplier sensitivity is increased by an order of magnitude as compared with the value adopted above, it is then possible to use $d \approx 1.3l_0 - 1.7l_0$ in measurements of the shower energy.

In any case, the estimates given here are only very approximate. They rely heavily on the adopted transparency of water, the sensitivity and size of the photomultipliers (threshold n_γ), and the geometric shape of the lattice. The effectiveness of the installation can be established reliably (after the values of the above parameters have been established with greater precision) by a standard Monte Carlo procedure.

B. Muon detection

In addition to the detection of the Čerenkov radiation due to the electromagnetic-nuclear showers, DUMAND also has to face the problem of recording single muons, both those produced in the installation and those arriving from outside.

At 10^{11}–10^{12} eV, the trajectory of a muon produced in the apparatus can be determined mainly from its direct Čerenkov radiation. The muon track is a continuous luminous cylinder. The flux of Čerenkov photons is independent of the muon energy and is equal to $n_\gamma = 200/2\pi r$ photon/cm^2 at a distance r (in cm) from the trajectory. For a detection threshold of $n_\gamma \sim 0.1$ photon/cm^2, the distance between the detectors should be $d \approx 2r \sim 6$ m. A muon of 10^{11}–10^{12} eV will also produce a number of showers in the installation due to bremsstrahlung radiation and pair production but, since the Čerenkov emission is highly directional, the probability that these showers will be recorded is quite small.

Muons with energy of 10^{13} eV can be detected and their energy measured by using showers due to electron–positron pairs created by the muon in the nuclear field.[8–9] The provisions made for the detection of these showers in the DUMAND project can be summarized as follows.

The main contribution to the muon energy losses resulting from pair formation is due to collisions in which the fraction of the muon energy transferred to the pairs is $f \sim m_e/m_\mu$. However, such collisions are relatively rare and the Čerenkov radiation from the resulting showers with energy $W_0 \sim (m_e/m_\mu)E$ usually misses the nearest detectors. The most effective energy transfers in muon detection are those in which the luminous shower segments coalesce, or almost coalesce, so that the radiation becomes continuous or quasicontinuous. This situation occurs for $f < m_e/m_\mu$ because the cross section increases with decreasing f. The minimum energy W_0 of a single cascade is determined by the threshold (for the given detector) flux of Čerenkov photons:

$$n_\gamma = \frac{10^2 W_0\,(\text{MeV})}{\sqrt{2}\,\pi d h}.$$

When $d \approx 20$ m and $W_0 \approx 1 \times 10^{10}$ eV, the lengths of the luminous segments of the cascade and the photon flux at a distance d are, respectively, $h \approx 2.4$ m and $n_\gamma \approx 0.5$ photon/cm^2. For $d \approx 20$ m and $W_0 \approx 10^9$ eV, we have $n_\gamma \approx 0.06$ photon/cm^2. Depending on the threshold flux ($n_\gamma = 0.05$ or 0.06 photon/cm^2), we may demand that $W_0 \geq 10^{10}$ eV or $W_0 \geq 10^9$ eV, and consider collisions with $f > W_0/E$. The cross section for the formation e^+e^- pairs, subject to the condition of complete screening, is given by

$$\sigma = \frac{16}{\pi}(\alpha Z r_0)^2 F(E) \ln \frac{m_e E}{m_\mu W_0}, \qquad (4)$$

where $r_0 = 2.8 \times 10^{-13}$ cm is the electron radius, $\alpha = 1/137$, Z is the atomic number, and

$$F(E) = \frac{7}{18}\left[\left(\ln \frac{m_e E}{m_\mu W_0} + \frac{10}{21}\right)\ln(183Z^{-1/3}) + \frac{\pi^2}{24} - \frac{1}{28}\right].$$

The cross sections and the mean free path λ of the muon in water are listed in Table I.

The condition that the radiation must be quasicontinuous can be written in the form $\lambda = 1/\sigma n \sim h$. It is clear from Table I that, in case I (threshold $n_\gamma = 0.6$ photon/cm^2), this condition is satisfied for $E \gtrsim 10^{14}$–10^{15} eV,

TABLE I.

E, eV	I		II	
	$W_0 = 10^{10}$ eV, $h = 2.4$ m		$W_0 = 10^9$ eV, $h = 1.8$ m	
	σ, cm^2	λ, m	σ, cm^2	λ, m
10^{13}	$8.6 \cdot 10^{-27}$	35	$4.2 \cdot 10^{-26}$	7.2
10^{14}	$4.2 \cdot 10^{-26}$	7.2	$1.1 \cdot 10^{-25}$	2.8
10^{15}	$1.1 \cdot 10^{-25}$	2.8		

whereas, in case II (threshold $n_\gamma = 0.06$ photon/cm^2), it is satisfied for $E \gtrsim 10^{13} - 10^{14}$ eV. When the continuity condition is reached (10^{14}–10^{15} eV), the intensity of the radiation emitted by the muon track becomes an excellent measure of the muon energy. In fact, the continuity condition is ensured for events with constant f (the cross section depends only on f). At the same time, $W_0 = fE$ increases with muon energy and there is a proportional increase in the intensity of the radiation emitted by the track. In individual cases, the cascades from the bremsstrahlung and from the photonuclear interactions of the muon may serve as an additional means of measuring energy.

C. Conclusions

We may summarize the above preliminary estimates as follows. Measurements of the Čerenkov radiation emitted by showers with energy between 10^{12} and 10^{15} eV or more can probably be carried out with lattice constant $d \sim 20$ m (for an absorption length $l_0 \sim 20$ m and photon threshold flux $n_\gamma \approx 0.6$ photon/cm^2) although measurements at low energies ($\sim 10^{12}$) are best carried out with a smaller cell.

For muons, there are two energy bands requiring different cell sizes. Energies of 10^{12}–10^{13} eV require $d \sim 6$ m for trajectory measurement. Determinations of the energies of individual muons are very difficult in this energy region. The muon energy spectrum can be measured mainly with the aid of showers due to bremsstrahlung photons. At energies of 10^{14}–10^{15} eV or more, a cell with $d \sim 20$ m is sufficient. Reliable measurements of both the muon trajectory and its energy are possible at these energies.

3. THE ATHENE PROGRAM: THE NEUTRINO-NUCLEON INTERACTION AT 1–100 TeV

A. Spectra of atmospheric neutrinos

The ATHENE program is concerned with experiments on atmospheric neutrons. (We use the word neutrino in the generalized sense which covers both the muon and electron neutrinos and the corresponding antineutrinos.) These neutrinos are produced in the decays of pions and kaons due to cosmic rays in the earth's atmosphere. At energies above 1 TeV, the main source of muon neutrinos are the $\pi^* \to \mu^* + \nu_\mu(\bar{\nu}_\mu)$ and $K^* \to \mu^* + \nu_\mu(\bar{\nu}_\mu)$ decays, and the main source of electron neutrinos are the less frequent decays $K^* \to \pi^0 + e^* + \nu_e(\bar{\nu}_e)$ and $K^0 \to \pi^* + e^* + \nu_e(\bar{\nu}_e)$. The muon neutrino flux is greater by a factor of about 20 as compared with the electron neutrino flux.

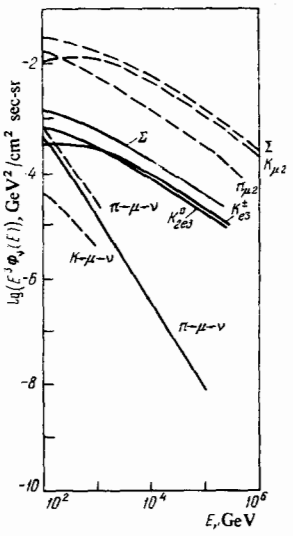

FIG. 3. Spectra of atmospheric neutrinos in the vertical direction. Dashed curves show the spectra of muon neutrinos; solid curves show the electron neutrinos. Spectra corresponding to different decay channels are shown (for example, $K_{\mu 2}: K \to \mu\nu$, $K_{e3}: K \to \pi e \nu$, and so on) as well as resultant spectra of muon and electron neutrinos (curves marked Σ).

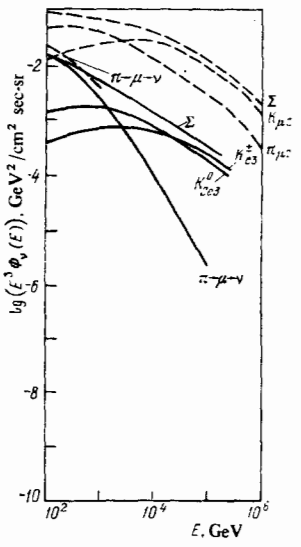

FIG. 4. Spectra of atmospheric neutrinos in the horizontal direction. Dashed curves show muon neutrino spectra; solid curves show the electron neutrino spectra. The figure also gives the spectra due to different decay channels, and the resultant spectra for muon and electron neutrinos (curves marked Σ).

The differential neutrino spectrum in the vertical direction for $E > 3$ TeV is characterized by the exponent $\gamma + 1 \approx 3.6$, whereas, in the horizontal direction, the spectrum is shallower and eventually reaches a power law with an exponent $\gamma + 1 \approx 3.6$ for $E \gtrsim 30$ TeV.

The horizontal neutrino flux is greater than the vertical flux: at 0.1 TeV, the two differ by a factor of three and at 100 TeV by a factor of ten. The difference between the spectral exponents and fluxes in the horizontal and vertical directions is due to the fact that the pions and kaons lose their energy in nuclear collisions prior to decay. In the horizontal direction, these particles move in a more rarefied atmosphere and are less likely to lose their energy prior to decay than in the vertical direction. The neutrino spectra in the vertical and horizontal directions have been calculated by L. V. Volkova and are shown in Figs. 3 and 4. The increase in the slope of the $K_{\mu 2}$ spectrum at about 5×10^{14} eV and the $\pi_{\mu 2}$ spectrum at about 2.5×10^{14} eV is due to the increase in the spectral exponent for the primary cosmic rays by $\Delta\gamma \approx 0.5$ above $\sim 3 \times 10^{15}$ eV. All the calculations are based on the assumption of a constant chemical composition of primary cosmic rays, based on measurements at $E \sim 10$ GeV/nucleon. However, the chemical composition of primary cosmic rays begins to vary for $E \gtrsim 10$ GeV/nucleon, and one cannot exclude the possibility that, even for $E \sim 10^{14}$ eV, the primary-radiation spectrum consists predominantly of nuclei. If this is to, the neutrino spectrum should be steeper than is shown in Figs. 3 and 4 at the lower energies. It is important to emphasize that the experiment will include measurements of the spectrum of at-

mospheric muons in a direction close to the vertical ($\theta \lesssim 30°$) up to energies $E \sim 10^{15}$ eV. This will enable us to carry out reliable calculations on the muon neutrino spectrum at these energies. It follows that calculations of the spectra of atmospheric neutrinos have, so far, been really only very rough estimates.

B. The neutrino–nucleon cross section at high energies (theoretical predictions)

The main aim of the ATHENE program is to determine the neutrino–nucleon cross section at 1–100 TeV. The cross section of the reaction $\nu_\mu + N \to \mu^- + \text{hadrons}$ has been measured in an accelerator experiment up to 160 GeV and is given by

$$\sigma = (0.83 \pm 0.11) \cdot 10^{-38} \; E \; \text{cm}^2, \tag{5}$$

where E is the neutrino energy in the laboratory system, expressed in GeV. The cross section for the reaction $\bar{\nu}_\mu + N \to \mu^+ + \text{hadrons}$ for $E < 40$ GeV is smaller than the cross section given by (5) by approximately a factor of three.

The linear increase in the cross sections for weak leptonic interactions ($\nu_\mu + e^- \to \mu^- + \nu_e$, $\nu_e + e^- \to \nu_e + e^-$, and so on) is a consequence of the fact that the interaction between the four particles participating in the reaction is a local "point" interaction. This is, of course, only an approximation and is merely an indication of the fact that the size of the interaction region (determined by the de Broglie wavelength of the particles in the center-of-mass system, i.e.,[3] $\lambda\!\!\!^{-}_c \sim 1/E_c$) is much greater than both the size of the particles themselves and their weak interaction range. If weak interactions are executed by the exchange of heavy W bosons, the interaction range is $r_W \sim 1/m_W$, where m_W is the mass of the W boson. For $\lambda\!\!\!^{-}_c \sim r_W$, the interaction cannot be regarded as a point interaction and the cross section ceases to increase rapidly with energy. If, on the other hand, the size of the particles participating in the reaction is $r_0 < r_W$, the cross section ceases to increase for $\lambda\!\!\!^{-}_c \sim r_0$ ($E_c \sim 1/r_0$).

The linear increase in cross section with energy should therefore cease at a center-of-mass energy E_c of the order of the mass of the W boson, or the reciprocal of the radius of one of the four particles participating in the reaction.

The center-of-mass energy is related to the laboratory energy through the formula $2Em = E_c^2$, where m is the mass of the particle at rest in the laboratory system.

According to modern ideas, the interaction between a high-energy neutrino and a nucleon is executed through the quasielastic scattering of the neutrino by the "point" components of the nucleon, i.e., partons or quarks. For example, the muon nuetrino is scattered by an n quark and transforms it into a p quark: $\nu_\mu + n \to p + \mu^-$. On the other hand, the antineutrino is scattered by a p quark: $\bar{\nu}_\mu + p \to n + \mu^+$. Hadrons are observed during the neutrino–nucleon collision ($\nu_\mu + N \to \mu^- + \text{hadrons}$), and recoil p quarks are created during subsequent collisions.

Not all transitions between quarks are of equal importance in weak-interaction theory. For example, the transition of a p quark into a "strange" λ quark is highly suppressed: the $\bar{\nu}_\mu + p \to \lambda + \mu^+$ cross section is smaller than the $\bar{\nu}_\mu + p \to n + \mu^+$ cross section by the factor $\sin^2 \theta_C$, where $\theta_C \approx 0.26$ is the Cabibbo angle.

In writing out the particular reactions, we have so far confined our attention to those cases in which the neutral lepton (neutrino) becomes a charged lepton: $\nu_\mu \to \mu^-$, $\nu_e \to e^-$. Such reactions are explained in terms of charged W-boson exchange and are generally regarded as occurring under the action of charged currents. If, on the other hand, the lepton does not change its charge state in the reaction ($\nu_\mu + N \to \nu_\mu + \text{hadrons}$), i.e., the neutrino undergoes neutral Z_0-boson exchange with the quarks, then it is said that the reaction occurs under the action of neutral currents. The neutral-current cross section for neutrino–nucleon scattering is about 30% of the charged-current cross section.

How far does the cross section (5) for neutron–nucleon interactions continue to increase? What is the expected cross section at the "ATHENE energies" of the neutrino (1–100 TeV)?

If the size of the quarks is less than the weak interaction range ($r_0 < r_W$), the increase in the cross section (5) will stop at $E_c \sim m_W$ in the center-of-mass system of the neutrino and the quark[4] or $E \sim m_W^2/2m_q$ in the

---

[3] We are using the system of units in which $\hbar = c = 1$ and the dimensions of length and time are the reciprocals of the dimensions of energy and mass, respectively. In particular, $1/m_p \approx 2.1 \times 10^{-14}$ cm, where m_p is the proton mass.

[4] Let us consider the change in the increase of the neutrino-nucleon cross section when the W boson of mass m_W is introduced. The neutrino-nucleon scattering cross section for a target with equal numbers of neutrons and protons in the quark parton model is given by

$$\sigma(s, m_W) = \frac{3}{2}\frac{G^2}{\pi}\int_0^1 dx\, N(x) \int_0^{sx} \frac{dQ^2}{[1+(Q^2/m_W^2)]^2} = \frac{3}{2}\frac{G^2 s}{\pi}\int_0^1 dx\, N(x)\frac{x}{1+(s/m_W^2)\,x}, \tag{6}$$

where the factor 3/2 is the mean number of p quarks (and n quarks) per nucleon, x is the fraction of the nucleon momentum in the center-of-mass system per quark ($0 \leq x \leq 1$), $N(x)$ is the probability that a quark in the nucleon will take up the fraction x of momentum (and, consequently, has the effective mass xm_N), $s = E_c^2$ is the square of the total energy of the neutrino and the nucleon in the center-of-mass system, s_x is the analogous quantity for the neutrino and the quark with momentum fraction x ($s_x = xs$), and $Q^2 = |q^2|$ is the square of the 4-momentum transferred from the leptons to the quarks.

Using the known form of $N(x)$, we can use (6) to show that the mass of the W meson reduces the cross section by a factor of two: $\sigma(s, m_W) = (1/2)\sigma(s, \infty)$ at $s/m_W^2 \approx 5$, i.e., at neutrino energy $E_\nu = m_W^2/2(m_N/5)$ in the laboratory system. This corresponds to the fact that the neutrino is scattered, on average, by a quark of mass $m_q \approx 200$ MeV. The same estimate for the quark mass $m_q = m_N \int_0^1 N(x)\,x\,dx = m_N \bar{x}$ is obtained by comparing the cross section (6) for $s \ll m_W^2$ with the experimental figure of $0.8 \times 10^{-38} E_\nu$ (5).

laboratory system, where m_q is the effective mass of the quark in the nucleon. If, on the other hand, $r_0 > r_W$, the neutrino–nucleon cross section will cease to increase for $E_c \sim r_0^{-1}$, whereas the cross section for the purely leptonic processes (for example, $\nu_\mu + e^- \to \mu^- + \nu_e$) will continue to increase up to $E_0 \sim m_W^2/2m_e$.

Let us begin by considering the first case ("point" quarks) in greater detail. In this case, the cross section (5) cuts off at $E_c \sim m_W$.

In renormalizable gauge theories of weak interactions, the mass of the W boson is a model-dependent quantity. In the generally accepted Weinberg–Salam model, the mass of the charged W boson is $m_W \approx 70$ GeV and the mass of the neutral boson is $m_Z \approx 80$ GeV. Berezinskiĭ and Smirnov[10] have considered "limiting" gauge models in which the effect of neutral currents is due to the exchange of a pair of charged W bosons. The mass of the W boson may amount to 500–800 GeV in this case. In the renormalizable theory of weak interactions involving the exchange of scalar mesons (Kummer and Segrè,[11] Shabalin,[12] and Segrè[13]), the mass of the intermediate mesons may be up to 300 GeV.

When the W-boson mass is $m_W = 70$ GeV, the "saturation" of the νN cross section occurs at neutrino energy $E_0 = m_W^2/2m_q \approx 12$ TeV, and for $m_W \approx 200$ GeV it occurs for $E_0 \approx 100$ TeV. Thus, the sharp change in the behavior of the cross section as a function of energy, which is particularly interesting from the point of view of existing theories, is well within the range of the ATHENE project.

Let us now consider the neutrino–nucleon cross section at energies of 1–100 TeV. To be specific, let us confine our attention to the muon neutrino, the flux of which from the atmosphere is much greater than the flux of electron neutrinos. The total cross section is due to the following reactions:

$$\nu_\mu + N \to \mu^- + \text{hadrons}, \tag{7}$$

$$\nu_\mu + N \to \nu_\mu + \text{hadrons}, \tag{8}$$

$$\nu_\mu + N \to L + \text{hadrons}. \tag{9}$$

The neutrino–electron scattering cross sections ($\nu_\mu + e^- \to \mu^- + \nu_e$, $\nu_\mu + e^- \to \nu_\mu + e^-$, $\nu_e + e^- \to \nu_e + e^-$, and $\bar{\nu}_e + e^- \to$ all) for $E < 100$ TeV are much less than the neutrino–nucleon cross section: for example, when $E \sim 100$ TeV, these cross sections are less than 10% of the total cross section for the Weinberg–Salam model.

At high energies, the cross section for the reaction given by (7) may also involve contributions due to the processes $\nu_\mu + n \to \mu^- + p_i$, where p_i are new heavy quarks with charge $+2/3$. The first of these is probably the charmed quark ($p_1 = c$). There is a similar possibility in the case of the cross section for the neutral currents in (8). The reaction given by (9) is hypothetical and involves the formation of new leptons L_j. This reaction can proceed both on n and p quarks, depending on the leptonic and electric charge of the L_j.

Thus, at energies much greater than the threshold for the production of new particles, one would expect that the total $\nu_\mu N$ cross section would take the form

$$\sigma \approx 1.2 \cdot 0.8 \cdot 10^{-38} \left(1 + \sum_i \operatorname{tg}^2 \theta_i + \sum_j \operatorname{tg}^2 \theta_j\right) E. \tag{10}$$

where the parameters θ_i and θ_j determine the possible suppression (or enhancement) of $n \to p_i$ and $\nu_\mu \to L_j$ transitions, and the coefficient 1.2 represents, very approximately, the contribution of the neutral currents to (8). The existence of the W boson leads to the replacement of E in (10) by $[(2m_q/m_W^2) + (1/E)]^{-1}$ and the saturation of the cross section for $E \gtrsim m_W^2/2m_q$. The weak logarithmic increase in the cross section at these energies is possible due to diffraction processes.

It follows that measurements of only the total neutrino–nucleon cross section at energies above 1–100 TeV may (1) lead to an indirect discovery of the existence of the W boson and the determination of its mass if $m_W \lesssim 200$ GeV, and (2) yield information on the existence of new particles and their contribution to the total neutrino–nucleon cross section. The latter may be established by comparing the cross section given by (5) at $E \lesssim 160$ GeV with the cross section (10) for $E > 1$ TeV.

Let us now consider possible measurements with the DUMAND system.

C. Apparatus and measurement program

The optimal (in our view) ATHENE program, which is possible for a large detector-lattice cell, involves the determination of the repetition frequency for showers produced by neutrino interactions in the installation, the determination of the shower energy and muon energy for $E_\mu \gtrsim 10$ TeV, and the determination of the direction of arrival of the primary particle.

In contrast to the more detailed program, which will be discussed below, we need not reconstruct here the kinematics of the particles after collision, which would involve measurements of angles less than 10 mrad; the precision with which the angles have to be measured in the "optimum" program is dictated only by the extent to which energy measurements depend on the relatively approximate determination of the direction of the shower axis. In the very preliminary estimate obtained in the last section, the required detector-lattice constant was $d \approx l_0 \approx 20$ m and, possibly, $d \approx 1.5 l_0$. From now on, we shall consider an installation having a volume of 10^9 m^3. This was discussed during the 1976 workshop on the DUMAND project.

In the "optimum" ATHENE program, it is possible to measure the cross sections for neutrino events with the formation of a muon (or several muons with energy in excess of 0.1–0.5 TeV), the fraction of energy carried off by the muon at muon energies above 10 TeV, and the cross section for muon-free events.

The installation should consist of a tetrahedral lattice of detectors (the cubic lattice is one of the least

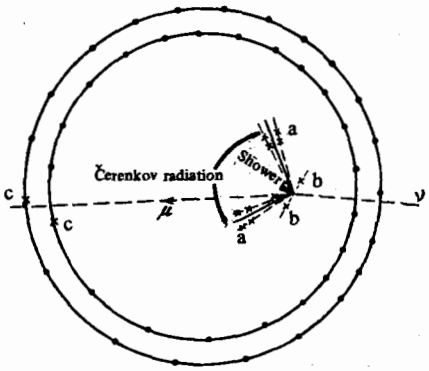

FIG. 5. Schematic representation of a neutrino event involving the production of a muon. The particle trajectories (neutrino, muon, and Čerenkov photons) are indicated by the dashed lines. The responding detectors are marked by crosses. a—Far-zone detectors (conical light layer); b—near-zone detectors (wide-angle emission); c—detectors in the muon module (spherical layer) illuminated by direct Čerenkov radiation due to the muon.

effective systems for the detection of Čerenkov radiation in the near zone), and a muon module surrounding the entire installation by a dense two-or three-layer array of photomultipliers viewing the inner volume of the system (Fig. 5). The distance between the photomultipliers in the muon module is determined by the requirement that the direct Čerenkov radiation of the muon leaving the installation has to be recorded. As shown above, this corresponds to $d \approx 6$ m. Each detector may have only one hemispherical photomultiplier with a field of view limited by the internal volume of the installation. To reduce the number of detectors, the muon module should be spherical in form (see Fig. 5). The muon module was suggested during the DUMAND-76 conference for somewhat different purposes by D. Cline.

A typical event produced by a neutrino with $E_\nu \approx 3$ TeV should appear as follows. During the $\nu_\mu + N \to \mu + \text{hadrons}$ reaction, a muon is emitted from the point of interaction and an electromagnetic-nuclear shower due to the hadrons develops. The neutrino will, on the average, transfer about half its energy to the muon ($E_\mu \approx 1.5$ TeV), the range of which in water exceeds 3 km. The muon will therefore be recorded in the muon module. Let us now consider the electromagnetic-nuclear cascade produced by the hadrons. The spatial coordinates of the center of the shower radiation will be roughly defined by the position of the detectors (b) in the near zone, and exactly defined by the time difference between the appearance of the signal in detectors (a) (conical layer) and (b). The position of this center, and the point at which the muon enters the muon module, will define the muon trajectory which, to within the required limits of accuracy, can be identified as the direction of motion of the neutrino and the direction of the axis of the electromagnetic-nuclear shower. In point of fact, the mean angles between the muon and the neutrino trajectories (θ_μ) and between the shower axis and the neutrino (θ_H) are equal: $\bar\theta_H = \bar\theta_\mu \approx \sqrt{2m_q/E_\nu} \approx 12$ mrad, where $m_q \approx 200$ MeV is the effective mass of the quark in the nucleon.[5)] It is clear from the angular distribution of the Čerenkov radiation (Fig. 1) that, to determine the shower energy, it is sufficient to know the position of the shower axis to within only 30–50 mrad. Still lower precision is required for the direction of the primary-neutrino trajectory to enable us to verify that it arrives along the direction for which the thickness of the material is much greater than the muon range. An independent determination of the direction of the shower axis is provided, although with lower precision, by the detector group (a) (conical layer) and the pulse heights from detectors (b). The latter and, to some extent, the pulse heights from detector group (a) can be used to determine the total shower energy E_H. For muon-free events, the direction of the shower axis can be determined only by recording the Čerenkov radiation. At muon energies in excess of 10 TeV, its track will be clearly seen throughout the volume of the installation, and the energy can be reliably determined from the pulse heights produced by detectors along the muon trajectory.

D. Frequency of neutrino events in the installation

We must now calculate the expected frequency of neutrino events and background events due to atmospheric muons (these calculations were carried out by L. V. Volkova). The calculations were based on the assumption that the linear growth (5) of the νN cross section was valid throughout the energy range, and without taking into account the creation of new particles. The re-

[5)] We shall write out the kinematic relationships for the deeply inelastic neutrino-nucleon scattering. We shall employ the usual kinematic and scaling variables: the square of the momentum transferred by the hadrons $Q^2 = |q^2|$, the muon energy E_μ, the total energy of the created hadrons E_H, the resultant momentum of the hadrons p_H, the energy transferred by the hadrons $\nu = E_\nu - E_\mu \approx E_H$, the scaling variable $x = Q^2/2m_N\nu$, which is the fraction of the total nucleon momentum in the center-of-mass system per quark (effective mass of this quark is therefore $m_q = xm_N$), and the fraction $y = \nu/E_\nu$ of the neutrino energy carried off by the hadrons. To calculate the angles θ_H and θ_μ, we shall use the well-known expression for Q^2 and the fact that the transverse momenta of the muon and the hadrons are equal:

$$Q^2 = 4E_\nu E_\mu \sin^2\frac{\theta_\mu}{2}, \quad p_H \sin\theta_H = p_\mu \sin\theta_\mu, \quad p_H \approx \sqrt{\nu^2 + Q^2}.$$

It is readily shown that

$$\sin^2\frac{\theta_\mu}{2} = \frac{Q^2}{4E_\nu E_\mu}, \quad \sin\theta_H \approx \sqrt{\frac{E_\mu}{E_\nu}\frac{\cos^2(\theta_\mu/2)}{1+(\nu^2/Q^2)}},$$

or, in scaling variables and for energy transfers that are not too small,

$$\theta_H \approx \sqrt{\frac{2m_N}{E_\nu}\frac{x(1-y)}{y}}, \quad \theta_\mu \approx \sqrt{\frac{2m_N}{E_\nu}\frac{xy}{1-y}},$$
$$\theta_H\theta_\mu \approx \frac{2m_N}{E_\nu}x.$$

The average values $\bar y = 1/2$ and $\bar x = 0.2$ (the latter follows from the form of the structure function in the neutrino-nucleon scattering process, or from a comparison of the sum of calculated cross sections for neutrinos on quarks with the magnitude of the measured νN cross section). For these values, we have

$$\bar\theta_H \approx \bar\theta_\mu = \sqrt{\frac{2m_N}{E_\nu}\bar x},$$

where $\bar x m_N$ is the effective mass of the quark.

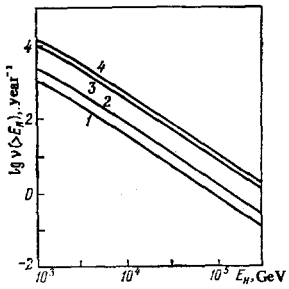

FIG. 6. Global spectra of neutrino showers. $\nu(>E_H)$—number of neutrino events per annum in which the energy release in electromagnetic-nuclear showers is greater than E_H: 1—for $\nu_e + N \to e^- +$ hadrons, $\bar{\nu}_e + N \to e^+ +$ hadrons (charged currents); 2—for $\nu_\mu + N \to \nu_\mu +$ hadrons, $\bar{\nu}_\mu + N \to \bar{\nu}_\mu +$ hadrons, $\nu_e + N \to \nu_e +$ hadrons, and $\bar{\nu}_e + N \to \bar{\nu}_e +$ hadrons (neutral currents); 3—for $\nu_\mu + N \to \mu^- +$ hadrons, $\bar{\nu}_\mu + N \to \mu^+ +$ hadrons (charged currents); 4) for the sum of all processes.

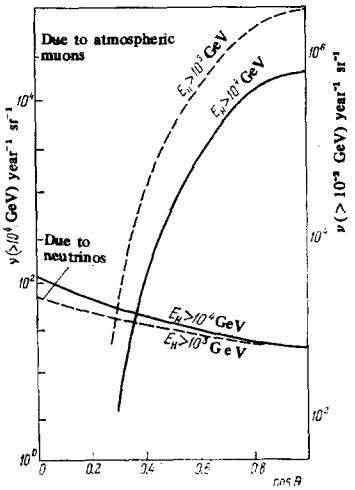

FIG. 8. Zenith-angle distribution of showers with energy greater than E_H due to muons and neutrinos. Dashed line shows the frequency of showers with $E_H \geq 1000$ GeV (right-hand scale); solid curve—$E_H \geq 10\,000$ GeV (left-hand scale).

duction in cross section for $E \gtrsim m_W^2/2m_e$ is the sought effect, and calculations performed for an unlimited increase in the cross section (5) in fact yield the upper mass limit below which the ATHENE program can be used to search for the W boson.

Figure 6 shows the global (integrated over all directions) spectra of showers with energy greater than E_H due to by neutrino interactions in the installation. The most frequent events are those due to the $\nu_\mu + N \to \nu_\mu +$ hadrons) and interactions involving the electron neutrinos ($\nu_e + N \to e +$ hadrons) produce roughly equal numbers of showers. This is so because the muon neutrinos, whose flux is greater than the flux of electron neutrinos by an order of magnitude, transfer only half their energy to the cascade whereas the entire energy of the electron neutrino is transferred to the cascade (through the electron and the hadrons). The global frequency of showers with energy greater than 10 TeV is 480 year^{-1}.

Showers produced in the installation by atmospheric muons form the background for the neutrino events. In contrast to the neutrinos, muons are absorbed in the

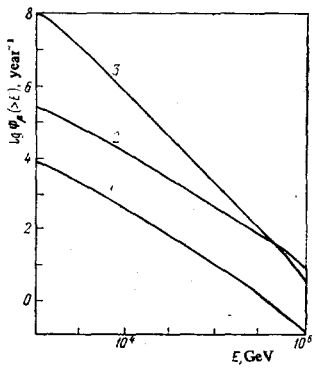

FIG. 7. Global spectra of muons. $\Phi_\mu(>E)$—number of neutrinos with energy greater than E that have passed through the installation: 1—muons created in $\nu_\mu N$ collisions inside the detection volume; 2—atmospheric muons created in direct generation events; 3—atmospheric muons created in π- and K-meson decays.

5-km layer of water above the installation and, therefore, the intensity of even the vertical muons is considerably reduced: by a factor of about 200 for muons of 1 TeV and about 70 for muons of 10 TeV.

Figure 7 shows the integrated (with respect to energy) global muon fluxes at a depth of 5 km in the ocean. This figure also gives the underwater spectrum of atmospheric muons of decay origin (pion and kaon decays) as well as muons created in the atmosphere as a result of the so-called direct generation (through decays of very short-lived particles). It is assumed in the calculations that direct production of muons in hadron collisions is about 10^{-4} of the production of pions. This follows from experimental data at energies below 100 GeV. The figure also shows the spectrum of neutrino-generated muons from the upper hemisphere inside the installation. For energies $E > 10^{13}$ eV, the flux of muons passing through the installation but created outside it exceeds by a factor of $1/(\gamma-1)\, bR\rho \approx 3.1$ the flux of neutrinos generated in the installation ($\gamma = 2.6$ is the exponent in the integrated neutrino spectrum, $b = (1/E)\,dE/dx \approx 3.2 \times 10^{-6}$ cm^2/g is the relative energy loss experienced by a muon in water, ρ is the density of water, and $R = 630$ m is the radius of the installation).

The main source of the "background" showers with a large energy release is the bremsstrahlung emitted by muons in the field of the nuclei ($\mu + Z \to Z + \mu + \gamma$). The high-energy γ ray produced in this reaction will generate an electromagnetic shower. The frequency of showers with energy $E_H \gtrsim 10$ TeV, initiated by muons in the vertical direction, is greater by a factor of about 1000 as compared with the neutrino-initiated showers.

Because of the exponential absorption of muons in the ocean, the background due to muon events decreases rapidly with increasing zenith angle θ (angle to the vertical). Figure 8 shows the frequency of showers due to muons and neutrinos as a function of the zenith angle. It is clear that, whereas the frequency of the "neutrino" showers increases with θ (due to the increase in the flux of horizontal neutrinos), the frequency of the "muon" showers decreases sharply (due to the absorption of muons). For $\theta \gtrsim 70$–$72°$, the frequency of neutrino showers for shower energies 1–10 TeV begins to

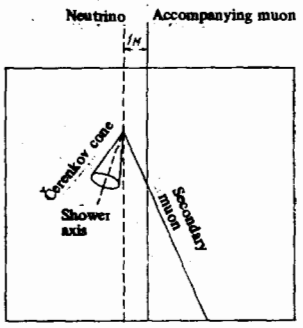

FIG. 9. Typical event produced by a vertical neutrino (according to D. Cline).

predominate over and above the frequency of muon showers.

Thus, in the horizontal direction ($\theta > 70°$) and in the upward direction, showers with total energy $E_H \gtrsim 1$–10 TeV are produced almost exclusively by the neutrinos. For an installation having a volume of 10^9 m^3, the frequency of neutrino showers with $E_H \gtrsim 10$ TeV in the horizontal direction ($70° \lesssim \theta \lesssim 90°$), and from the lower hemisphere, amounts to $\nu \approx 390$ year^{-1}. For showers with $E_H \gtrsim 1$ TeV, the corresponding frequency is $\nu \approx 9.700$ year^{-1}.

E. Program of detailed studies of the interaction process

During the DUMAND-76 Conference, D. Cline outlined a program for a detailed study of the neutrino–nucleon interaction that was similar to the procedure adopted in experiments using accelerators. In contrast to the "optimum" program, which we have discussed, the Cline program provides, in addition to measurements of the shower energy and the angle θ_H, the further measurements of both θ_μ and θ_H (which amount to $\lesssim 10$ mrad) and the energy of even the low-energy muons. The Cline program devotes particular attention to events produced by vertical neutrinos. Figure 9 illustrates schematically a typical neutrino event of this kind ($E_\nu \approx 10$ TeV). (This figure is taken from Cline's paper). The neutrino (broken line) produces a muon and an electromagnetic-nuclear shower with average emission angles $\bar{\theta}_H \approx \bar{\theta}_\mu = \sqrt{2m_q/E_\nu} \approx 6$ mrad as a result of the $\nu_\mu + N \to \mu +$ hadrons reaction. The vertical solid line, parallel to the neutrino trajectory, represents the trajectory of a muon created in the atmosphere in the same pion or kaon decay as the recorded neutrino. The trajectory of the partnering muon establishes with sufficient accuracy the direction of arrival of the neutrino (θ_ν). Thus, Cline suggests that the vertical neutrino event can be identified on the basis of: (1) the Čerenkov emission of the shower, (2) the muon produced during the interaction, and (3) the trajectory of the partnering muon near (~1 m) the axis of the hadron shower. The measured quantities are: the angles θ_H, θ_μ, and θ_ν (using the trajectory of the partnering muon) and the energies E_H and E_μ (the energy of the primary muon should be based on measurements on showers produced by bremsstrahlung and the pair production process). Once θ_H, θ_μ, θ_ν, E_H, and E_μ are known, it is possible to reconstruct the kinematics of the event and to investigate the distribution in y (fraction of energy carried off by the hadrons). Direct determination of θ_ν is impossible in the horizontal and upward directions. Multimuon events can be investigated by recording muons of all energies.

Our preliminary estimates show that angle measurements to within 1–3 mrad, as provided for in the Cline program, and measurements of the energy and trajectory of the muon with $E_\mu \lesssim 1$ TeV with the aid of photomultipliers located inside the installation, will require a detector-lattice cell of not more than 5 m so that a large number of photomultipliers for the 10^9 m^3 installation is unacceptable. However, as noted by Cline himself, this parameter can be determined more accurately by the Monte Carlo method. Moreover, the number of vertical neutrino events accompanied by a partnering atmospheric muon will be very small (for $E_\nu \sim 10$ TeV, this amounts to about 2% of all the neutrino events). This is explained as follows.

The angular distribution of muons at the depth of 5 km decreases sharply with increasing zenith angle (Fig. 10), and at $\theta \approx 45°$ the muon flux is lower by a factor of two as compared with the vertical flux. This leaves the small solid angle $\Delta\Omega \sim 2$ sr for neutrino events accompanied by the atmospheric muons.

Moreover, because of the steepness of the spectra of decaying pions and kaons, the spectrum of atmospheric neutrinos is formed during the emission of the neutrinos at a mean angle $\alpha = 55°$ ($\overline{\cos\alpha} = 0.57$) to the direction of motion of the decaying particle. The ratio of the muon and neutrino energies in the laboratory system is then readily seen to be given by

$$\frac{E_\mu}{E_\nu} = 0.64 \cdot \frac{0.43m^2 + 1.57m_\mu^2}{m^2 - m_\mu^2},$$

where m is the mass of the kaon or pion. For kaon decays, this ratio is equal to about 0.3. For $E_\nu = 10$ TeV, the energy of the partnering muon formed during the decay of the kaon is, on the average, 3 TeV. The range of this muon in water is about 5 km so that, as a rule, it will not reach the installation. Moreover, the flux of kaon neutrinos from the atmosphere at the energy of 10 TeV is greater by a factor of three as compared with the flux of pion neutrinos. These two facts lead to the above estimates.

Finally, we must add that the background of bremsstrahlung muons, which is very high for the vertical direction, ensures that it is practically impossible to ob-

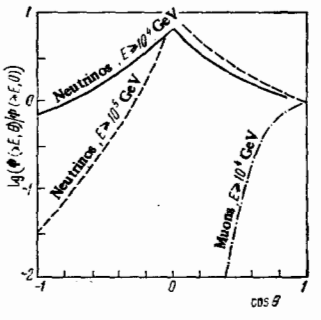

FIG. 10. Angular distribution of muons of atmospheric origin and of neutrinos at a depth of 5 km in the ocean. θ is the angle with the vertical (zenith angle).

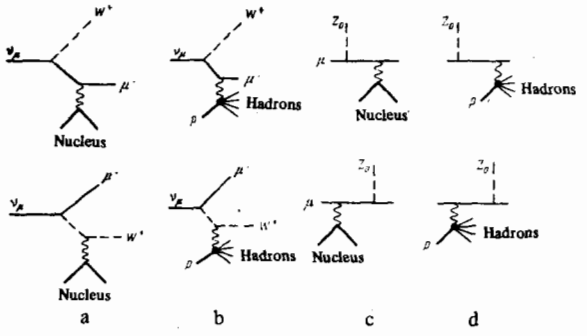

FIG. 11. Graphs of the creation of W and Z_0 bosons in the reactions $\nu_\mu + Z \to Z + \mu^- + W^+$ (graph a), $\nu_\mu + p \to \mu^- + W^+ +$ hadrons (b), $\mu + Z \to Z + \mu + Z_0$ (c), and $\mu + p \to \mu + Z_0 +$ hadrons (d).

serve showers from the muon-free neutrino interaction, and this greatly impedes the observation of the small number of neutrino events involving the creation of a muon (estimated above). For $E \approx 10$ TeV, the installation is traversed by about 1 million muons per annum, and the number of showers with $E_H \gtrsim 10$ TeV produced by muons within the solid angle $\Delta\Omega \sim 2$ is 20000 per annum.

The number of photomultipliers employed in the installation can be reduced by abandoning observations of vertical events and viewing only the inner part of the installation with the detectors in the muon module.

We have concentrated our attention on the differences between the programs but, of course, most of the ground covered by them is common.

F. The search for the W boson

The defect of the ATHENE program as a whole is that direct production of W bosons cannot be observed (this is corrected in the UNICORN program).

The creation of a charged W boson and neutral Z_0 boson in the neutrino and muon beams occurs in the following reactions (Fig. 11)

$$\nu_\mu + Z \to Z + \mu^- + W^+,$$
$$\nu_\mu + p \to \mu^- + W^+ + \text{hadrons},$$
$$\mu + Z \to Z + \mu + Z_0,$$
$$\mu + p \to \mu + Z_0 + \text{hadrons},$$

where Z represents the Coulomb field of the nucleus and p is a proton.

The above reactions are characterized by the fact that the ratio of the W-boson energy to the energy of the muon in the final states is, on the average, given by $E_W/E = m_W/m_\mu$. This is why, in the detailed version of the program, the creation of the W boson could be deduced, as noted in Cline's paper at the DUMAND-76 conference, from events in which practically the entire neutrino energy is transferred to hadrons (in the $W \to$ hadrons decay), or from the production of muon pairs (in the $W \to \mu\nu$ decay) in which one member has a high energy and the other a low energy.

However, the number of events involving the production of a W boson in the DUMAND experiment is too low for this analysis.

The cross section for the coherent production of the W boson in the Coulomb field of the nucleus is given by

$$\sigma_W = \alpha^2 G \frac{Z^2}{A} F(\beta, m_W) = 2.3 \cdot 10^{-37} \frac{Z^2}{A} F(\beta, m_W) \quad \text{n}^2/\text{nucleon}, \quad (11)$$

where $\beta = 2E_\nu/Rm_W^2$ and $R \approx 0.29A^{1/3} \times 10^{-13}$ cm represents the linear dimensions of the nuclear formfactor for $A = 16$, $m_* = 1/R = 0.27$ GeV.

For asymptotically high energies, $F(\beta, m_W)$ is given by the analytic formula[14a]

$$F(\beta, m_W) = \frac{1}{4\sqrt{2}\pi}\left[\frac{2}{3}\ln^3\beta + \frac{61}{6}\ln^2\beta + \left(-\frac{31}{3} + \frac{88}{\beta} + \frac{64}{3}\ln Rm_W\right)\ln\beta - \left(\frac{304}{9} - \frac{64}{\beta}\right)\ln Rm_W - \frac{12}{\beta} - \frac{40}{9}\pi^2 - \frac{1.33}{1.08} + 32\left(\frac{1}{3} + \frac{1}{4\cdot 2^2} + \frac{1}{5\cdot 3^2} + \ldots\right)\right]. \quad (12)$$

At intermediate energies, the calculations were not carried out for large W boson masses ($m_W > 30$ GeV).

The asymptotic state is reached very slowly, especially when the finite mass of the muon is taken into account.[14b] Comparison of the asymptotic formula with exact calculations[14c] shows that the values of β for which the asymptotic situation is reached increase with increasing m_W. This means that the use of the asymptotic formula with finite β produces an overestimate for the W-boson production cross section.

In the Weinberg model ($m_W \approx 70$ GeV) with $\beta = 10$ ($E_\nu = 100$ TeV), the cross section calculated from the asymptotic formula is $\sigma_W \approx 8 \times 10^{-36}$ cm^2/nucleon and the frequency of neutrino events involving the creation of the W boson is $\nu_W \approx 0.2$ year^{-1}. An appreciable reduction in the cross section occurs for energies $E_\nu < 100$ TeV ($\beta < 10$).

The optimum neutrino energy in the search for the light W boson in the ATHENE program is $E_\nu \sim 20$ TeV. If the W boson decays into a muon and a neutrino, the event is a muon pair production in which one of the muons has the low energy $(m_\mu/m_W)E_\nu \sim 3 \times 10^{10}$ eV and is not recorded by the installation, and the other has the average energy $E_\mu \sim 10$ TeV and is reliably recorded (muon energy $\gtrsim 10$ TeV, which defines the choice of the neutrino energy $E_\nu \gtrsim 20$ TeV). The mass of the W boson should not then exceed $\sqrt{2Em_*/10} \approx 30$ GeV. In the model based on four colored quarks, the probability of $W \to \mu\nu$ decay is 1/8 of the total probability and, consequently, the cross section for the production of a single muon inside the installation is $\sigma_{W\to\mu} \sim 1 \times 10^{-36}$ cm^2/nucleon, whereas the total number of such events in the horizontal direction ($\theta > 70°$) and in the upward direction is $\nu_{W\to\mu} \sim 2$ year^{-1} (about 50 muons with $E_\mu \gtrsim 10^{13}$ eV will then pass through the installation in the same direction per annum). In the decay of the W boson into hadrons, the "loss" of the low-energy muon ensures that the event becomes indistinguishable from $\nu_\mu + N \to \nu_\mu +$ hadrons and $\nu_e + N \to e +$ hadrons. It seems, therefore, that a search for even the light W boson is impossible in this experiment.

G. Main conclusions

1) Atmospheric neutrinos can be recorded at energies between 1 and 100 TeV. A detector lattice with cell size $d \approx 20$ m (absorption length for light in water $l_0 \approx 20$ m) and the muon module can be used to measure the following: the direction of arrival of the neutrino, the coordinates of the point of intersection, shower energy, the detection of one or more muons with energy of 0.3–10 TeV (created during the interaction between neutrinos and the installation), and the energies and trajectories of muons with energies in excess of 10 TeV.

In the detection of the neutrino interactions, it is best to confine the experiment to the upward directions and zenith angles $\theta \geq 70°$ in the upper hemisphere in which the background due to atmospheric muons is low. The expected number of neutrino-initiated showers in these directions for a linear increase in the cross section and an installation of 10^9 m^3 is $\nu \sim 9700$ year^{-1} for $E_H \gtrsim 1$ TeV, and $\nu \sim 390$ year^{-1} for $E_H \gtrsim 10$ TeV.

2) Measurement data can be used to obtain the following physical results:

— At energies of 1–100 TeV, the neutrino–nucleon cross section can be measured up to energies at which the cross section ceases to increase linearly with energy.

— Measurements can be carried out of the cross section for muon-free events (by recording the muons in the muon module) due to neutral currents and the interaction of electron neutrinos.

— Cross sections for reactions resulting in the formation of several muons can be measured.

— For energies $E > 10$ TeV, when muons cannot be recorded through pair production, the experiments will yield the distribution over the fraction of energy transferred to hadrons.

— The slowing down in the cross section can be used to establish, at least indirectly, the existence of the W boson and to estimate its mass if it does not exceed 150–200 GeV.

Any excess of the cross section at $E \sim 1$ TeV over and above the linear extrapolation (5) will contain information about new particles.

If the cross section is low in comparison with the linear extrapolation (5), and increases slowly with energy for $E \gtrsim 1$ TeV, this will be evidence that the mass of the W boson is low, or quarks are not point particles.

4. UNICORN PROGRAM: EXPERIMENTS WITH EXTRAGALACTIC NEUTRINOS ABOVE 10^{14}–10^{15} eV

The UNICORN program has the following aims:

1) Search for distant cosmological epochs at which bursts of high-energy cosmic rays were produced (high-energy neutrino astronomy).

2) Search for the W boson with mass between 30 and 100 GeV, using the Glashow resonance reaction $\bar{\nu}_e + e^- \to W^- + \text{hadrons}$.

3) Determination of the neutrino–nucleon cross section at 10^{14}–10^{16} eV.

4) In the case of sufficiently high fluxes of extragalactic neutrinos, investigation of the elementary neutrino–nucleon interaction: distribution over y (fraction of energy transferred to hadrons), detection of νN interactions with the formation of several muons, and detection of muon-free events.

The UNICORN program rests on a review of two very different questions, namely, the sources of high-energy neutrinos and the possibility of studying the interaction between neutrinos and matter.

It would appear at first sight that, since it is not possible to predict accurately the flux of extragalactic neutrinos, there is little point in discussing the possibility of studying them with the aid of elementary interactions. However, it will be shown below that it is basically possible to determine separately the neutrino flux and the cross section for its interaction with nucleons and electrons.

A. Sources of extragalactic neutrinos and expected fluxes

The main source of cosmic neutrinos are the decays of pions produced in collisions of cosmic-ray protons with nuclei in the interstellar and intergalactic gas, or with photons. The former will be referred to as pp neutrinos and the latter as $p\gamma$ neutrinos.

The $p\gamma$ neutrinos are of maximum interest and are created during collisions between protons and remnant photons. The remnant radiation is due to distant cosmological epochs when the universe was hotter. The density and energy of the remnant photons, determined by the radiation temperature T, are known for each cosmological epoch with red shift z. At present ($z = 0$), the temperature is $T = 2.7\,°$K, the density of photons is $n = 390$ cm^{-3}, and the mean photon energy is $\omega_{\text{rem}} = 6.3 \times 10^{-4}$ eV. For an epoch with a red shift z, the photon density and mean energy should be higher than they are now by factors of $(1+z)^3$ and $(1+z)$, respectively.

A collision between a proton and a remnant photon is conveniently considered in the reference frame in which the proton is at rest. The energy of the incident proton in this system is $\omega_r \approx \Gamma\omega$, where $\Gamma = E_p/m_p$ is the Lorentz factor of the proton and ω is the energy of the remnant photon in the laboratory system. At present ($z = 0$), protons with $E \geq 3 \times 10^{19}$ eV lose their energy in interstellar or intergalactic space mainly by the production of pions during collisions with remnant photons. For energies $E \lesssim 3 \times 10^{20}$ eV, the proton energy losses are mainly due to collisions with photons in the high-energy "tail" of the Planck distribution, and the production of pions occurs at threshold photon energies of about 150–200 MeV in the rest system of the proton. The pion photoproduction cross sections at these energies are well known.

To determine the flux of extragalactic $p\gamma$ neutrinos, it is therefore necessary to know only the fluxes of cosmic rays in other galaxies. The cosmic-ray spectrum has been determined directly only in our own galaxy: it

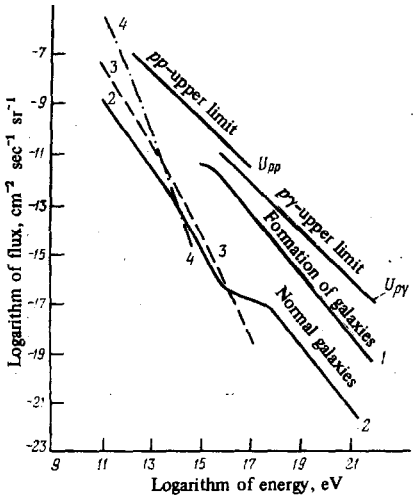

FIG. 12. Integrated spectra of cosmic neutrinos. U_{pp} and $U_{p\gamma}$ represent the upper limits for pp and $p\gamma$ neutrino fluxes; 1—neutrino spectrum based on the model calculations[16]; 2—spectrum of neutrinos from normal galaxies; 3—galactic spectrum of neutrinos (in the direction of the center of the galaxy), and 4—spectrum of atmospheric neutrinos.

extends to energies in excess of 10^{20} eV. Our galaxy belongs to the so-called normal class of galaxies and is a relatively typical radio source in its own class.

The fluxes and spectra of pp and $p\gamma$ neutrinos produced by cosmic rays in normal galaxies have been calculated[15] and are shown in Fig. 12. The calculated fluxes contain a number of uncertainties (especially in the case of the pp neutrinos), and it may well be that the real fluxes will be substantially lower.

The presence of strong extragalactic sources (quasars, Seifert galaxies, and radiogalaxies), and the great variety of observational material indicating a higher activity of galaxies (including our own) in the past, undoubtedly indicate a higher output of cosmic rays and, therefore, neutrinos as well. However, the possibilities in this area are not unlimited: there is a strict upper limit to the flux of neutrinos at high energies.[15,16] This restriction is based on the fact that neutral pions are produced simultaneously with charged pions in pN and $p\gamma$ collisions. The γ rays produced during their decay initiate the electromagnetic cascade which develops due to collisions with remnant cascade The entire energy of the primary γ ray or electron is thus transformed into x-ray or γ-ray emission that can be observed. This provides an upper limit on the neutrino flux. The U_{pp} and $U_{p\gamma}$ curves in Fig. 12 show the upper limits for the pp and $p\gamma$ neutrino fluxes.

B. Neutrinos from distant cosmological epochs

Let us now directly consider the experimental data that provide indirect evidence for the existence of powerful extragalactic sources of cosmic rays and for their enhanced activity in the past.

Supernova explosions[17] are probably the main source of cosmic rays. High-mass clouds evolve more rapidly than low-mass clouds and, therefore, one would expect an increase in the rate of production of massive stars (and, consequently, of supernova explosions) in the past. This is confirmed by a variety of observations. The production of elements in our galaxy (and especially the production of iron which occurs in supernova envelopes) requires[18] an increase in the frequency of supernova explosions in the past. Detailed results can be obtained by analyzing the abundance of heavy elements in the stellar atmospheres in giant elliptic galaxies.[19] Analysis of correlations between the color indices of galaxies and the frequency of supernova explosions also confirms an increase in the frequency of supernova explosions in that past.[20]

There is reliable evidence[21] for the so-called cosmological evolution of powerful radiogalaxies and quasars, the net effect of which is an increase in their output and number per unit volume of the universe with increasing red shift z. It is natural to suppose that these objects are powerful sources of cosmic rays.

We have so far confined our attention to data indicating a "smooth" evolution of sources. Against this background, there is the expected discontinuous increase in the rate of production of massive first-generation stars. This discontinuity may occur during an early stage of evolution of galaxies near the epoch of their formation (this is the so-called bright phase). The increase in the frequency of supernova explosions during this stage ($2 \leqslant z \leqslant 10$) has been discussed by Schwarts, Ostriker, and Yahil.[22] They came to the conclusion that energy release in the form of kinetic energy is possible during the explosions of supernovas. This release is of the order of 10^{61} erg in a galaxy of mass 10^{11} M. (Our galaxy has a mass of 1.8×10^{11} M.). This energy release leads to[16] a neutrino flux in the region of the upper limit in Fig. 12.

A burst in cosmic-ray production during the formation of primary galaxies or during primary star-formation has also been suggested.[16] This burst is thought to have occurred for $z\approx 30$ and continued for about 10^7 years. The total energy release in cosmic rays is $\sim 5\times10^{60}$ erg, i.e., of the same order as predicted by Schwarts *et al.*[22] The burst hypothesis[16] explains the observed isotropic x-ray and γ-ray emission (both the flux and the spectral features, with certain discrepancies at the very highest energies). The neutrino flux predicted by this model is shown in Fig. 12 (curve 1).

C. Neutrinos emitted by early envelopes of supernovas

The dense supernova envelopes around early pulsars may act as another source of high- and ultrahigh-energy neutrinos.[23a]

Gunn and Ostriker[24] have proposed a mechanism for the acceleration of protons and nuclei to high energies, based on high-intensity magnetodipole radiation of an early pulsar.

They consider a neutron star formed during the ejection of the envelope after a supernova explosion and assume that the rotational axis of the star is not parallel to the magnetic moment (this is the inclined-rotator model of a pulsar). An object of this kind is a source

of magnetodipole radiation, the frequency of which is equal to the rotational frequency Ω of the pulsar. The magnetodipole radiation "sweeps out" the gas from the immediate neighborhood of the pulsar, and an empty cavity appears in the space between the pulsar and the ejected envelope. Charged particles from the stellar magnetosphere are trapped by the magnetodipole wave, and rapidly assume a velocity of the order of the velocity of light. They traverse the vacuum cavity in phase with the wave. The result of this is that the particles are accelerated until the Lorentz factor reaches $\Gamma \sim (\omega_H/\Omega)^{2/3}$, where $\omega_H = eH_r/mc$ is the Larmor frequency in the wave zone. This mechanism ensures that, at each instant of time, all particles of a given type that have passed through the evacuated cavity have the same energy, and this energy decreases as the pulsar "ages." According to the estimates given by Gunn and Ostriker, the pulsar in the Crab object was responsible for the acceleration of protons up to 3×10^{17} eV in the course of its creation. The estimate given in[25] was that the pulsar could accelerate protons up to 2×10^{21} eV.

There are other known mechanisms for the acceleration of charged particles by a pulsar. These are connected with the interaction of the magnetodipole wave with the plasma in the ejected envelope,[26] and with the relativistic stellar wind[27] leaving the star. The attractiveness of pulsars as sources of cosmic rays rests on the possible transformation of the enormous rotational energy of the neutron star into the energy of the magnetodipole radiation which, in turn, can be transformed with high efficiency into the energy of relativistic particles.

An expanding envelope around an early pulsar, into which accelerated protons are continuously injected, has also been considered[23a] (Fig. 13). The high density of the envelope during the early stages of the expansion ensures that the protons lose their energy mainly through the production of pions in nuclear encounters. In a very dense envelope, the pions multiply in further collisions until the pion mean free path is comparable with its decay mean free path. Neutrinos and γ rays are produced in the pion decay chain.

In accordance with observational data, it was assumed[23a] that the mass of the envelope was $M \sim M_\odot$ and that the envelope expanded with velocity $u \sim 10^9$ cm/sec. Three characteristic times can be distinguished in the history of the expanding shell:

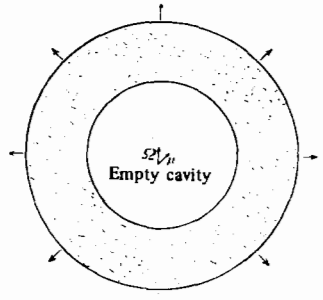

FIG. 13. Expanding envelope of a supernova filled with cosmic rays and surrounding an early pulsar.

1) The instant of time beyond which the decay time of charged pions with Lorentz factor Γ becomes less than the nuclear collision time:

$$t_\pi(\Gamma) = \left(\frac{3M\sigma_\pi c\tau_\pi}{4\pi m_H u^3}\right)^{1/3}\Gamma^{1/3} = 1.9\cdot10^2\Gamma^{1/3} \text{ sec}; \quad (13)$$

where $\sigma_\pi \approx 2.5\times10^{-26}$ cm^{-2} is the πN interaction cross section, $\tau_\pi = 2.6\times10^{-8}$ sec is the lifetime of a charged pion at rest, and $m_H = 1.7\times10^{-24}$ g is the mass of the hydrogen atom.

2) The instant of time beyond which the envelope becomes transparent to γ rays:

$$t_\gamma = \sqrt{\frac{3M}{4\pi u^2 \varkappa_{\text{rad}}}} = 2.8\cdot10^6 \text{ sec}; \quad (14)$$

3) The instant of time beyond which adiabatic losses by protons in the envelope begin to predominate over nuclear-collision losses:

$$t_a = \sqrt{\frac{3(1-\alpha^\gamma)M\sigma_p}{4\pi m_H u^3}} \approx 1.3\cdot10^7 \text{ sec}; \quad (15)$$

where $\sigma_p \approx 4\times10^{-26}$ cm^2 is the pN interaction cross section, $\alpha \approx 1/2$ is the fraction of energy retained by a proton on collision, and γ is the integral exponent of the cosmic-ray spectrum in the envelope.

For $t < t_a$, the entire energy of the protons injected by the pulsar is thus transformed into pions; for $t > t_a$, the energy is expended mainly in work done during the expansion of the shell (adiabatic losses). During the time $\tau_\gamma = t_a - t_\gamma$, the envelope is a source of γ radiation, whereas during the time $\tau_\nu = t_a - t_\pi$, it is a neutrino source. It is interesting to note that, if the injection of accelerated particles decreases rapidly with time, and becomes negligible for $t_0 \lesssim t_\gamma$, the envelope becomes a pure neutrino emitter with emission time $\tau_\nu = t_0 - t_\gamma(\Gamma)$, where Γ defines the energy of the radiated neutrinos.

The neutrino flux from the supernova envelope is a model-dependent quantity and contains a number of unknown factors.

Consider, for example, the Gunn-Ostriker model for the pulsar in the Crab nebula.[24]

The initial magnetodipole luminosity of the Crab is estimated to be $L_0 = 4.8\times10^{45}$ erg/sec. It continues to decrease for 80 years due to radiative-gravitational deceleration of the pulsar in accordance with the law $L(t) = L_0/[1 + (t/\tau_g)]$, where $\tau_g = 1.4\times10^4$ sec. At the same time, the proton energy decreases as $E(t) = E_0/[1 + (t/\tau_g)]^{1/3}$, where $E_0 = 3\times10^{17}$ eV. Neutrinos with energy $E_\nu \sim 10^{11}$ eV (detection threshold for the DUMAND project) are produced during the decay of pions with energies $E_\pi \sim 4\times10^{11}$ eV. These pions begin to decay intensively in the envelope at $t_\pi(4\times10^{11} \text{ eV}) \approx 3\times10^3$ sec. The neutrino radiation thus becomes detectable for $t \gtrsim t_\pi$. During this stage, the pion energy undergoes fragmentation in the envelope until the pions reach the decay energies. At $t \approx 4\times10^5$ sec, pions with the maximum energy begin to decay (this is accompanied by the emission of neutrinos with maximum energy $\sim 9\times10^{15}$ eV). Beyond this point, the neutrino energy decreases because

of the reduction in the initial energy of the proton. Between $t_\pi \approx 3\times10^3$ and $t_a \approx 1.3\times10^7$ sec, a proton will transfer between 20 and 50% of its energy to neutrinos (a muon loses a very small part of its energy as a result of collisions per decay). If we suppose that the mean fraction of transferred energy is 30%, the total energy of the neutrino radiation is

$$W_\nu \approx 0.3\int_{t_\pi}^{t_a} \frac{\lambda L_0}{1+(t/\tau_g)}\,dt = 0.3\lambda L_0\tau_g \ln\frac{t_a}{\tau_g} \approx \lambda 1.3\cdot10^{50}\ \text{erg}, \qquad (16)$$

where λ is the fraction of the magnetodipole luminosity transferred to the accelerated particles.

The high-energy neutrinos (between 10^{15} and 9×10^{15} eV) are emitted during the period between $t=4\times10^5$ sec and $t_a=1.3\times10^7$ sec, and the energy carried off by them is $W_\nu \approx \lambda\times6\times10^{49}$ erg.

The γ rays are emitted between $t=2.8\times10^6$ sec and $t_a=1.3\times10^7$ sec, and the total energy of this radiation is $W_\nu \approx \lambda\times3\times10^{49}$ erg.

The resultant flux of neutrinos with energies in excess of 10^{15} eV, due to all pulsars of this type throughout the history of the universe is

$$\Phi_\nu = \frac{1}{4\pi}\frac{W_\nu}{\bar{E}_\nu}\nu_{SN}cT_{Mg}\xi\eta = \lambda\xi\eta\cdot2\cdot10^{-12}\ \text{cm}^{-2}\ \text{sec}^{-1}\ \text{sr}^{-1}, \qquad (17)$$

where $\bar{E}_\nu \approx 3\times10^{15}$ eV is the mean neutrino energy, $\nu_{SN} \approx 0.01\ (\text{Mpc}^3\times100\ \text{year})^{-1}$ is the frequency of supernova explosions within the limits of the local supercluster,[28] $T_{Mg}=1.3\times10^{10}$ year is the age of the universe, ξ is the fraction of pulsars of the type under consideration, and η is the evolution factor representing the possible increase in the frequency of supernova explosions in the past. The limit on the flux (17) due to the presence of γ radiation is close to the U_{pp} curve in Fig. 12.

If, instead of the radiative-gravitational deceleration of the pulsar, we use magnetodipole deceleration $L(t) = L_0[1+(t/\tau)]^{-2}$ with $\tau \approx t_a$ in the model we are considering, the resultant energy of the emitted neutrinos and the flux given by (17) have to be increased by a factor of about 10.

Thus, in addition to the model dependence, the resultant flux of neutrinos from the pulsar envelopes depends on the product of three factors representing the fraction (λ) of the energy of magnetodipole radiation of the pulsar that is transferred to the accelerated particles, the fraction (ξ) of pulsars of the given type, and the possible considerable increase in the frequency of supernova explosions in the past.

The predicted neutrino flux from distant extragalactic supernova explosions will also depend on λ and ξ. In the optimistic variant, the neutrino radiation from a supernova explosion is possible in the DUMAND project at distances of 10–15 Mpc.

The detection of γ radiation from early supernova envelopes is more effective.[23b] Such observations may well provide important information on the possibilities of supernova envelopes as neutrino sources.

D. Detection of neutrinos and studies of weak interactions in the UNICORN program

The fluxes of pp neutrinos produced under cosmic conditions are characterized by the fact that, in all cases (including dense supernova envelopes), muons of practically any energy will succeed in decaying. This means that the flux of electron antineutrinos ($\bar{\nu}_e$) amounts to 1/6 of the total flux. If the mass of the W boson lies between 30 and 100 GeV, most of the neutrino events at energies between 10^{15} and 10^{16} eV in the DUMAND installation will be due to the Glashow resonance reaction[29]: $\bar{\nu}_e + e^- \to W^- \to$ hadrons. With good resolution, these events will appear as a narrow peak in the shower spectrum at the energy $E_H = E_0 \equiv m_W^2/2m_e$. Measurements of E_0 can, therefore, be used to determine the mass of the W boson.

This does not, however, exhaust the importance of observations of resonance events. The frequency of resonance events in the installation can be used to determine unambiguously the flux of the antineutrinos $\bar{\nu}_e$ which, for the pp neutrinos, is directly related to the flux of the muon neutrinos. This offers a possibility of measurements of the cross section for the $\nu_\mu + N \to \mu$ + hadrons reaction, which is of particular interest because, if the mass m_W is known, the magnitude of this cross section contains information about the point nature of quarks, or the creation of new quarks. For example, if the cross section is small and the W boson mass is large, this will probably mean only that the quarks are not point particles.

The $p\gamma$ neutrino fluxes are depleted in $\bar{\nu}_e$. This is so because pion production occurs mainly at the threshold of the $p+\gamma_{rem} \to n+\pi^+$ reaction, and electron antineutrinos are not produced in the π^+ decay chain. The electron antineutrinos are produced in fluxes of $p\gamma$ neutrinos from protons of higher energy, and from muon decays produced during collisions between high-energy γ rays and remnant photons: $\gamma+\gamma_{rem} \to \mu^+ + \mu^-$. The result is that the fraction of the electron antineutrinos in the resultant p neutrino flux is reduced by an order of magnitude as compared with the pp neutrinos, and the detection of the resonance peak for a large W boson mass ($m_W \gtrsim 70$ GeV) becomes difficult because of the presence of background neutrino events.[6)]

The p neutrinos with energies $E \gtrsim 3\times10^{15}$ eV (curve 1 in Fig. 12) can be recorded by the DUMAND installation with high efficiency because of the large energy release, using both the electromagnetic-nuclear showers inside the installation and the muons produced outside the installation. Figure 14 shows the efficiency of the DUMAND system for the detection of neutrinos, using only showers inside the installation due to the νN interactions. The region above the $\nu=10$ and $\nu=1$ yr^{-1} curves gives the neutrino fluxes to be recorded by

[6)] The situation is radically modified if there are neutrino oscillations,[30] i.e., in the presence of $\bar{\nu}_\mu \rightleftarrows \bar{\nu}_e$ ($\nu_\mu \rightleftarrows \nu_e$). In our case, these transitions, which occur at very long distances (of the order of the size of the universe), should lead to the same $\bar{\nu}_\mu$ and $\bar{\nu}_e$ fluxes, amounting to 1/6 of the total neutrino flux.

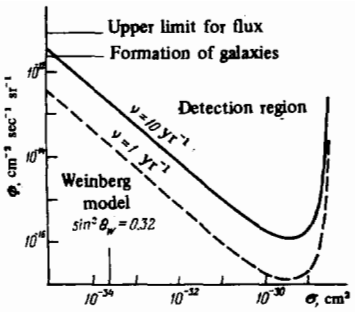

FIG. 14. Neutrino flux to be detected by the DUMAND installation of volume 10^9 m^3 as a function of neutron-nucleon cross section when the frequency of events is $\nu=1$ year^{-1} and $\nu=10$ year^{-1}. For given cross section, the detected flux is determined by the coordinates of points lying above the corresponding curves. The thin lines indicate the upper limit of the $p\gamma$ neutrino flux, the flux of $p\gamma$ neutrinos in the Berezinskiĭ–Zatsepin model,[16] and the cross section at $E=3.4\times10^{15}$ eV in the Weinberg model.

DUMAND at the level of more than 10 and more than 1 events per year, respectively, for the cross section defined by the abscissa of the chosen point. When all events are taken into account, including muons produced outside the system, the two curves lie lower by a factor of about 4 as compared with Fig. 14.

The neutrino–nucleon cross section for the $p\gamma$ neutrino at energies above 3×10^{15} eV can be estimated[16] from the absorption of neutrinos arriving from the other side of the earth.

We must now consider the above effects in greater detail.

E. Detection of *pp* neutrinos and search for the *W* boson

Let us now consider possible ways of searching for the W boson.[31] The energy of electron antineutrinos producing the resonance reaction $\bar\nu_e+e^-\to W^-+$hadrons, when the W boson mass is 30 and 100 GeV, is 9×10^{14} eV and 10^{16} eV, respectively. The mass of the W boson in the Weinberg model ($m_W\approx70$ GeV) corresponds to $E_0=m_W^2/2m_e=5\times10^{15}$ eV. The cross section for the $\bar\nu_e+e^-\to W^-+$hadrons reaction near resonance is given by the Breit-Wigner formula

$$\sigma=\frac{4\pi}{m_W^2}\,\frac{2J+1}{2j+1}\,\frac{\Gamma_l\Gamma_h}{(E_c-m_W)^2+(\Gamma^2/4)}, \tag{18}$$

where $J=1$ is the spin of the W boson, $j=1/2$ is the electron spin, E_c is the total energy in the center-of-mass system, $\Gamma_l=(1.6\pi\sqrt2)\,Gm_W^3$ is the width of the leptonic decay channel $W+l+\nu$, Γ_h is the width of the hadron decay channel, and Γ is the total width. In the four-quark color model (p, n, λ, and c is a charmed quark), we have $\Gamma_h\approx6\Gamma_l$ and $\Gamma_h\approx3\Gamma/4$ if there are only two leptonic channels: $W\to e\nu$ and $W\to\mu\nu$.

When the mass of the W boson is $m_W\gtrsim30$ GeV, the entire upper hemisphere above the installation is transparent to the antineutrinos with resonance energy $E_0=m_W^2/2m_e$. Using (18), we can easily find for a power law-spectrum of $\bar\nu_e$ the frequency of resonance events in the installation with a total number N_e of electrons:

$$\nu_{res}=3\sqrt2\,\pi^2\gamma N_eG\Phi_{\bar\nu_e}(>E_0), \tag{19}$$

where $\Phi_{\bar\nu_e}(>E_0)$ is the flux of the $\bar\nu_e$ with energy in excess of E_0, γ is the exponent in the integrated antineutrino spectrum, and $G=10^{-5}/m_p^2=4.4\times10^{-33}$ cm^2 is the cross section corresponding to the Fermi weak-interaction constant.

Equation (19) shows that the number of resonance events is uniquely determined (for the power-type spectrum) by the integrated flux of antineutrinos at energy above the resonance value, and this exhausts the dependence of ν_{res} on the mass of the W boson. This important point enables us to calibrate the installationfor flux: by measuring the frequency of appearance of resonance events, we can obtain the integrated flux of antineutrinos at energy in excess of the resonance value.

Let us consider (19) in greater detail. The frequency of resonance events is $\nu_{res}\sim\Phi_{dif}(E_0)\,\Gamma_{lab}\sigma_{max}$, where $\Phi_{dif}(E_0)$ is the antineutrino flux differentiated with respect to energy, $\Gamma_{lab}=(m_W/m_e)\,\Gamma\sim Gm_W^4/m_e$ is the width of the resonance in the laboratory system, and $\sigma_{max}\sim1/m_W^2$ is the cross section at the resonance maximum. Since the resonance neutrino energy is $E_0=m_W^2/2m_e$, and for power-law spectra $\Phi_{dif}(E_0)\,E_0\sim\Phi(>E_0)$, we can verify that the frequency of appearance of resonance events is, in fact, independent of the mass of the W boson.

The frequency of appearance of resonance events ν_{res}(year^{-1}) with energy release $E_H=m_W^2/2m_e$ in the DUMAND system of volume V (expressed in m^3) is related to the integrated flux of antineutrinos $\Phi_{\bar\nu_e}(E_0)$ by the formula

$$\Phi_{\bar\nu_e}(>E_0)=5\cdot10^{-15}\,\frac{\nu}{10}\cdot\frac{10^9}{l}\ \text{cm}^{-2}\ \text{sec}^{-1}\ \text{sr}^{-1}. \tag{20}$$

In the case of *pp* neutrinos, the electron antineutrinos comprise 1/6 of the total flux[7)] and, consequently, the "threshold" flux of all the neutrinos (for $\nu=10$ events per annum) when the DUMAND installation has a volume of 10^9 m^3 is 3×10^{-14} cm^{-2} sec^{-1} sr^{-1}. In the Weinberg model ($m_W\approx70$ GeV), this flux must be available at energy $E_0=5\times10^{15}$ eV. Figure 12 shows that this is greater by two orders of magnitude than the resultant flux of neutrinos for normal galaxies (curve 2).

At energies in excess of 10^{15} eV, the background due to atmospheric muons and neutrinos is negligible, and, in the case of a resonance production of the W boson, there is the further background of other events, also due to cosmic neutrinos. The background processes are the following: $\nu_\mu+N\to\mu+$hadrons, $\nu_\mu+N\to\nu_\mu+$hadrons, $\nu_e+N\to\nu_e+$hadrons, $\nu_e+N\to e_e+$hadrons, $\nu_e+e\to\nu_e+e$, $\nu_\mu+e\to\nu_\mu+e$, and $\nu_\mu+e\to\mu+\nu_e$. The width of a resonance amounts to only 5–6% of the resonance energy E_0, and the energy resolution of DUMAND will substantially exceed this width. The condition for the detection of the W boson will, therefore, be that the frequency of resonance events must be greater than the frequency of back-

[7)] In the presence of neutrino oscillations,[30] the fraction is 1/4.

ground showers from the upper hemisphere with energy release in excess of E_0. When all the above reactions are taken into account, the ratio of the frequency of resonance events to the frequency of appearance of background showers turns out to be[31]

$$\frac{\nu_{res}}{\nu_{backgr}(>E_0)} = 1.3\cdot 10^3 \left(\frac{10}{m_W}\right)^2, \quad (21)$$

where m_W is measured in GeV. This result can be improved if, in addition, we isolate background events by recording the high-energy muon and use only events inside the energy interval ΔE corresponding to the resolution of the system.

F. Detection of $p\gamma$ neutrinos

As already noted, $p\gamma$-neutrino fluxes are depleted in electron antineutrinos as compared with the pp neutrinos. This means that the ratio given by (21) is reduced by roughly an order of magnitude for $p\gamma$ neutrinos if there are no neutrino oscillations. Nevertheless, bearing in mind the discrimination against muon events, and using events only within the resolution interval ΔE of the system, one would hope to be able to detect a W boson with mass up to 70 GeV.

In addition, the $p\gamma$ neutrino can be detected in reactions involving the production of muons:

$$\nu_\mu + N \to \mu + \text{hadrons}, \quad \nu_\mu + e \to \mu^- + \nu_e, \quad (22)$$

and in muon-free reactions with the production of electromagnetic-nuclear showers:

$$\left.\begin{array}{c} \nu_e + N \to e^- + \text{hadrons}, \quad \nu_\mu + N \to \nu_\mu + \text{hadrons}, \\ \bar{\nu}_\mu + N \to \bar{\nu}_\mu + \text{hadrons}, \\ \nu_e + N \to \nu_e + \text{hadrons}, \quad \nu_e + e \to \nu_e + e, \quad \nu_\mu + e \to \nu_\mu + e, \\ \bar{\nu}_\mu + e \to \bar{\nu}_\mu + e. \end{array}\right\} \quad (23)$$

The p-neutrino flux predicted by the model considered by Berezinskiĭ and Zatsepin[16] is $\Phi_\nu = 2.4\times 10^{-12}$ cm^{-2} sec^{-1} sr^{-1} at energies above 3.4×10^{15} eV. Muons produced by these neutrinos in the reactions defined by (22) have energies in excess of 10^{15} eV and should be reliably detected by the system.

The integrated flux of muons from the reactions defined by (22) and occurring outside the installation is given by

$$\Phi_\mu = \frac{2}{3}\Phi_\nu \frac{\sigma_0}{\gamma n_N b}\left(\ln\frac{E}{E_0} + \frac{1}{\gamma}\right); \quad (24)$$

where $\sigma_0 = (3/2)(G^2/\pi)\, m_W^2 \approx 1\times 10^{-34}$ cm^2 is the neutrino–nucleon cross section at saturation (we are considering a target with equal numbers of neutrons and protons so that, on the average, the nucleon has 3/2 of a p quark and 3/2 of an m quark). Next, we suppose that, when $E_0 \sim 3\times 10^{14} - 5\times 10^{14}$ eV (for $m_W \approx 70$ GeV), the cross section begins its logarithmic increase due to the interaction with low-momentum quarks in the nucleon[32] (diffraction scattering of the neutrino by the nucleon); $b = (1/E_\mu)\,dE_\mu/dx = 3.2\times 10^{-6}$ cm^2/g is the muon absorption coefficient of water and γ is the exponent in the integrated neutrino spectrum.

The frequency with which the muons pass through the installation (when they are produced outside the system) is 250 year^{-1}, the muon production frequency inside the installation is 80 year^{-1}, and the resultant frequency of showers in the installation due to the processes defined by (23) is 94 year^{-1}. The resultant frequency of detection of neutrino events in the model[16] for $m_W \approx 70$ GeV should be about 430 year^{-1}; in the absence of the logarithmic increase in the cross section ($\sigma_{\nu N} \sim 10^{-34}$ cm^2), the resultant frequency is about 180 year^{-1}.

Measurements of cross sections in the $p\gamma$-neutrino flux are possible because of both the resonance creation of the W boson (for $m_W \leq 70$ GeV) and the absorption of the neutrinos in the earth, which begins for $\sigma \gtrsim 2.5\times 10^{-34}$ cm^2.

Reliable detection of high-energy muons can be used in the identification of muon-free events and events involving the creation of one or more muons, and to determine the fraction of energy carried off by the muons.

G. Main conclusions

1) High-energy cosmic neutrinos are produced during collisions of cosmic-ray protons with nuclei in the interstellar and intergalactic gas (pp neutrinos) and with remnant photons ($p\gamma$ neutrinos). The neutrino emission due to cosmic rays from normal galaxies sets the lower limit for the neutrino flux. The upper limit is due to x-ray and γ-ray emission, which accompanies the neutrino emission and should not exceed the observed value. Model calculations, based on the enhanced activity of cosmic objects in the past, can lead to neutrino fluxes much greater than the flux from normal galaxies.

Dense envelopes of supernovas surrounding early pulsars may act as powerful sources of high energy ($10^{14} - 10^{16}$ eV) pp neutrinos. Their resultant flux may be close to the upper limit for pp neutrinos. Neutrino emission from individual extragalactic sources of this type may also be detectable. The strength of the neutrino sources in the early supernova envelopes may be established by studying their γ-ray emission.

2) Among all the high-energy particles, the universe is transparent only to the neutrinos. The problem for high-energy neutrino astronomy is to search for distant cosmological epochs during which a cosmic-ray production burst took place. The flux of these neutrinos at the epoch with red shift z is directly related to the contemporary ($z = 0$) $p\gamma$-neutrino flux because the density and energy distribution of target particles (remnant photons) and the cross sections for the formation of pions in collisions between protons and remnant photons are known for each epoch.

3) A search for the W boson with mass between 30 and 100 GeV is possible in the pp-neutrino fluxes. The existence of the W boson should be reflected in the resonance behavior of the $\bar{\nu}_e + e^- \to W^- \to$ hadrons reaction which leads to the appearance of a burst in the electromagnetic-nuclear shower spectrum at the energy $E_H = m_W^2/2m_e$ within the energy interval ΔE defined by the resolution of the installation.

Moreover, this process can also be used to calibrate the installation for flux because, according to (20), the

flux of electron antineutrinos is determined by the resonance value of the shower frequency. It is known that it is possible to determine the cross sections for other neutrino processes which, when taken in combination with the measured mass of the W boson, provide information on the existence of new leptons and quarks, or the effective radius of the quarks. The observation of muon-free neutrino events, and neutrino events with the creation of one or more muons, is possible because of the efficient detection of high-energy muons.

At high energies, when the cross sections exceeds 2.5×10^{-34} cm^2, the neutrino-nucleon cross section can be estimated from the absorption of neutrinos in the earth. [16]

5. ACOUSTIC METHOD OF DETECTING HIGH-ENERGY NEUTRINOS

Askar'yan and Dologoshein[33] and, independently, Bowen[34] proposed, during the DUMAND-76 conference, the use of an acoustic method for the detection of neutrinos with energies in excess of 10^{16} eV at a great depth in the ocean.

The advantage of the acoustic method of detection as compared with the optical method lies in the much greater absorption of sound in water ($R\sim1000$ m) as compared with the absorption of light in water ($l_0\approx20$ m). This means that a much greater volume of seawater can be used for detection purposes. In contrast to Bowen's proposal, [34] Askarjan and Dologoshein[33] consider the coherent generation of sound, resulting in the propagation of an acoustic wave within a thin disk perpendicular to the neutrino trajectory, so that it is possible to determine the direction of arrival of the particle (without distinguishing between the two opposite senses of the motion along the trajectory).

The emission of acoustic waves during the passage of a charged particle through a medium was first discussed by Askar'yan in 1957. [35] The sound generation mechanism described in[35] is connected with the formation of microbubbles and local hot-spots in the medium along the charged particle track. Volovik and Lazurik-Él'-tsufin[36] subsequently considered the thermoacoustic mechanism due to the uniform heating of the medium along the particle trajectory, which occurs as a result of ionization. The acoustic radiation emitted during the propagation of charged particles in solids has been detected experimentally. [37] The acoustic method of detection was proposed by Volovik and Khristiansen[38] for the detection of cosmic-ray particles. [6)]

Let us consider, following mainly the discussion given by Askar'yan and Dolgoshein, [33] the acoustic detection method for neutrinos with energies in excess of 10^{16} eV in water.

High-energy neutrinos produce electromagnetic-nuclear showers in the medium. Near the shower maximum, where a large quantity of electrons with energies equal to the critical value or less is formed, the ionization heating of a narrow channel along the shower axis takes place. The radius of this channel is determined by the transverse-distance distribution of the electrons relative to the shower axis, and the effective channel diameter d_{eff} at high energies may be of the order of a few centimeters. The length of the heated part of the channel can be estimated as in Chap. 2, and the result is $h\approx3\sqrt{\ln E_0/\varepsilon}$ (in t-units). The heating of the channel produces its expansion and hence the appearance of an acoustic wave. Coherent generation occurs at wavelengths λ such that $\lambda>d_{eff}$. The angle θ to the normal to the shower axis, within which the coherent emission takes place, is determined by the usual interference condition $h\sin\theta\lesssim\lambda$. A cylindric acoustic wave is thus found to propagate in the plane perpendicular to the shower axis and is centered on a shower segment of length h. The size of the wave layer at right-angles to the wave vector is determined by the length h of the heated part of the shower and the coherence angle θ. In the nearwave zone, $r<h^2/\lambda$, the expansion of the wave layer due to the angular divergence is small, and the wave occupies a cylinder of base area $\pi h^4/\lambda^2$. This cylinder lies in the plane perpendicular to the shower axis, and its generators (length $\sim h$) are parallel to this axis. The flux of energy through the lateral walls of the cylinder at a distance r from the shower axis is inversely proportional to the area $2\pi rh$ and, consequently, the pressure due to the acoustic wave in the near-wave zone falls off as $1/\sqrt{r}$.

The frequency spectrum of the emission is determined by the time profile of the pulse exciting the oscillations (sharp increase in the volume of the heating channel followed by smooth compression during cooling) and the general conditions governing the propagation of the wave in the compressible fluid. [39] The frequency spectrum is of the form λ^{-2} and is cut off (because of the coherence condition) on the short-wavelength side for $\lambda\sim d_{eff}$. The effective pressure due to the coherent acoustic emission is due to wavelengths $\lambda\sim d_{eff}$. Askar'yan and Dolgoshein[33] have estimated the effective acoustic-wave pressure in the near zone due to the electromagnetic-nuclear shower of energy Q:

$$P_{\text{eff}}\approx0.1\frac{Q}{Q_0}\frac{1}{\sqrt{r}}; \tag{25}$$

where P_{eff} is measured in dyn/cm^2, the distance r is in cm, $Q_0=10^{16}$ eV, and the effective dimensions of the radiating part of the shower are taken to be $h\approx5$–6 m and $d_{eff}=1$ cm (the corresponding wavelength is $\lambda\sim1$ cm and frequency $f\sim25$ kHz). The optimum frequency band for detection from the point of view of the sound absorption length (about 1000 m for seawater) and acoustic noise in the ocean lie in the band $f\sim20$–30 kHz. As the frequency is reduced, the absorption length increases, but this is accompanied by a sharp increase in the noise in the ocean. The minimum neutrino energy defined by these conditions has been estimated[33] as being 10^{16} eV.

In November 1976, a group of physicists headed by L. R. Sulak carried out a test experiment on the de-

[6)] This is not intended to be an exhaustive summary of published information on the acoustic detection of particles and we may well have missed previous or more important work.

tection of the acoustic emission in water due to a narrow proton beam from the Brookhaven accelerator in the USA.

They used protons of 200 MeV with $5\times10^{10}-5\times10^{12}$ protons per pulse, and protons of 32 GeV with $3\times10^{11}-3\times10^{12}$ particles per pulse. The beam had a diameter of about 6 cm and was allowed to enter a tank filled with water. The distance traversed by the beam in the tank was about 30 cm. Two hydrophones were used and their distance from the beam could be varied between 1 and 10 m. Measurements showed that the pressure was directly proportional to the energy lost by the beam and, for $E\sim10^{20}$ eV, exceeded the calculated value[33] by a factor of 10. We shall not discuss here all the data obtained as a result of this test experiment. At the time of writing, these were preliminary results and we merely note that the sound generated by the beam could be detected simply by listening. It is important to remember, however, that the efficiency with which the acoustic emission is generated in this particular experiment may be connected with the formation of microbubbles, and this may well be suppressed at a great depth in the ocean.

Let us now note the characteristic features of acoustic emission that are important for underwater detection of high-energy neutrinos[33]:

Radiation is generated in a coherent fashion so that the pressure due to the acoustic wave is directly proportional to the shower energy and hence to the neutrino energy.

The effective frequency of the acoustic radiation is determined by the transverse size of the shower and amounts to $f\sim25$ kHz at very high energies.

In the near wave zone, the emission occupies the volume of a thin disk of thickness h (length of radiating part of shower) and radius R (sound absorption length). The plane of the disk is perpendicular to the shower axis. This means that the direction of arrival of the neutrino can be determined with very high precision. The length of the acoustic pulse ($\sim10^{-5}$ sec) may turn out to be an important characteristic for the separation of the useful signal from the background of acoustic noise in the ocean. An underwater installation in the form of a parallelepiped with base area of 10×10 km and height of 1 km has been proposed[33] for the detection of neutrinos with energies $E_\nu\gtrsim10^{16}$ eV. The system should contain 100 000 hydrophones distributed uniformly throughout the volume (10^{11} m^3). The increase in the volume of the installation by two orders of magnitude as compared with the 10^9 m^3 envisaged for the optical variant of DUMAND should extend very substantially the possibilities of the neutrino experiments based on the UNICORN program (in particular, it should facilitate the search for the W boson in pp neutrino fluxes from normal galaxies). The improvement in the angular resolution of the system ($\sim1^\circ$) and the increased sensitivity ensure that the installation can be used as a "neutrino telescope" for the observation of neutrino radiation from early supernova envelopes.

The threshold energy of the detected neutrinos is a critical question for the acoustic method. This energy depends on the distribution of electrons with transverse distance from the shower axis and, mainly, on the efficiency with which the acoustic oscillations are generated at a great depth in the ocean as well as the level of acoustic noise in the ocean.

6. CONCLUSIONS

Studies of cosmic neutrinos with energies in excess of 10 TeV can be used to obtain important information for neutrino physics. This refers, firstly, to the study of weak interactions in fluxes of atmospheric neutrinos and, secondly, to the detection of extragalactic neutrinos with energies in excess of 100 TeV (high-energy neutrino astronomy) and studies with the aid of weak interactions at energies that will remain inaccessible to accelerators constructed in the foreseeable future. We are satisfied that underwater experiments, of which the DUMAND project is a particular example, will be an adequate means of investigating cosmic neutrinos. These experiments are essentially a gigantic version of accelerator neutrino experiments. The detector is the ocean supplied with the detecting elements (optical and acoustic), and the low intensity of the neutrino beam is effectively compensated by the great volume of the detector. In contrast to previous cosmic experiments, the proposal is to observe directly the elementary interactions within the volume of the detector, rather than record particles at a large distance from the point of interaction.

The DUMAND project is distinguished by the complementary character of its two programs. On the one hand, provisions have been made for the study of weak interactions using atmospheric neutrinos whose flux, up to a few tens of TeV, can be detected relatively reliably, and, on the other hand, the project involves experiments with extragalactic neutrinos which, given a positive result, will provide very important and unique information both for astrophysics and for elementary-particle physics. If the result is negative (with an installation of 10^9 m^3), this will merely give cause to the mournful arguments by the astrophysicists, who will undoubtedly find many "natural" explanations for the low flux of extragalactic neutrinos.

We have given moderately optimistic estimates of the possibilities of cosmic-neutrino physics and high-energy neutrino astrophysics. In some ways, they are based on an extrapolation from experimental data, and are our own intuitive ideas. Nevertheless, we think that the structure of nature is more complex and far richer than we imagine today and that, when the past of the Universe is viewed through the "neutrino window," the result may well be exceedingly surprising.

[1]F. Reines, H. Gurr, W. Kropp, *et al.*, Proc. Intern. Seminar on Neutrino Physics and Astrophysics, Vol. 1, Moscow, 1969, p. 25; S. Krishnaswamy, M. G. K. Menon, *et al.*, *ibid*, p. 9.
[2]Yu. N. Vavilov, L. N. Davitaev, Yu. A. Trubkin, and V. M.

Fedorov, Izv. Akad. Nauk SSSR Ser. Fiz. **34**, 1997 (1970).
[3]L. V. Volkova and G. T. Zatsepin, Yad. Fiz. **14**, 211 (1971) [Sov. J. Nucl. Phys. **14**, 117 (1972)].
[4]V. L. Ginzburg and S. I. Syrovatskiĭ, Proiskhozhdenie kosmicheskikh lucheĭ (The Origin of Cosmic Rays), AN SSSR, M., 1963 (English translation published by Pergamon Press, Oxford, 1964).
[5]Proc. 1975 Summer Workshop on DUMAND, ed. by P. Kotzer, Western Washington State College, 1976.
[6]A. A. Belayev, I. P. Ivanenko, and V. V. Makarov, in: Proc. Workshop DUMAND-76, ed. by A. Roberts, FNAL, Batavia, 1977, p. 563.
[7]A. Roberts, in: Proc. Conf. Neutrino-76 (to be published).
[8](a) I. S. Alekseev and G. T. Zatsepin, in: Mezhdunarodnaya konferentsiya po kosmicheskim lucham (Moskva 1959) [International Conference on Cosmic Rays (Moscow 1959)], Izd. AN SSSR, M., 1960, p. 320. (b) T. Kitamura, K. Mitsui, *et al.*, in: Proc. Fourteenth Intern. Cosmic Ray Conf., Vol. 6, Munich, 1975, p. 2145.
[9]S. Miyake, as in Ref. 6, p. 257.
[10]V. S. Berezinskiĭ and A. Yu. Smirnov, as in Ref. 6, p. 35.
[11]W. Kummer and G. Segrè, Nucl. Phys. **64**, 585 (1965).
[12]E. P. Shabalin, Yad. Fiz. **9**, 1050 (1969) [Sov. J. Nucl. Phys. **9**, 615 (1969)].
[13]G. Segrè, Phys. Rev. Lett. **33**, 1244 (1974).
[14](a) G. von Gehlen, Nuovo Cimento **30**, 859 (1963); (b) V. M. Pizh, in: Problemy yadernoĭ fiziki i kosmicheskikh lucheĭ (Problems in Nuclear Physics and Cosmic Rays), No. 2, Vishcha Shkola, Kharkov, 1975, p. 45; (c) B. W. Brown and J. Smith, Phys. Rev. D **3**, 207 (1971).
[15]V. S. Berezinsky and A. Yu. Smirnov, Astrophys. Space Sci. **32**, 461 (1975).
[16]V. S. Berezinsky and G. T. Zatsepin, as in Ref. 6, p. 215.
[17]V. L. Ginzburg, Dokl. Akad. Nauk **92**, 1133 (1953).
[18]D. D. Clayton and J. Silk, Astrophys. J. Lett. **158**, L43 (1969).
[19]J. P. Ostriker and T. X. Thuan, Astrophys. J. **202**, 353 (1975).
[20]B. M. Tinsley, Publ. Astron. Soc. Pacific **87**, 837 (1975).
[21]M. S. Longair, Mon. Not. RAS **133**, 421 (1966); M. Schmidt, Astrophys. J. **176**, 273 (1972).
[22]J. Schwarts, J. P. Ostriker, and A. Yahil, *ibid.* **202**, 1 (1975).
[23]V. S. Berezinskiĭ and O. F. Prilutskiĭ (a) cit. in Ref. 6, p. 229; (b) Pis'ma Astron. Zh. **3**, No. 4 (1977) [Sov. Astron. Lett. **3**, No. 4 (1977)].
[24]J. E. Gunn and J. P. Ostriker, Phys. Rev. Lett. **22**, 728 (1969).
[25]M. Grewing and M. Heintzmann, Phys. Rev. Lett. A **42**, 345 (1973).
[26]R. M. Kulsrud *et al.*, Phys. Rev. Lett. **28**, 636 (1972).
[27]M. J. Rees and J. E. Gunn, Mon. Not. RAS **167**, 1 (1974).
[28]G. A. Tammann, in: Supernovae and Supernova Remnants, ed. by C. B. Cosmovici, Reidel, Dordrecht, 1974, p. 155.
[29]S. L. Glashow, Phys. Rev. **118**, 316 (1960).
[30]B. M. Pontecorvo, Zh. Eksp. Teor. Fiz. **53**, 1717 (1967) [Sov. Phys. JETP **26**, 984 (1968)].
[31]V. S. Berezinskiĭ and A. Z. Gazizov, Pis'ma Zh. Eksp. Teor. Fiz. **25**, 276 (1977) [JETP Lett. **25**, (1971)].
[32]B. L. Ioffe, Usp. Fiz. Nauk **110**, 357 (1973) [Sov. Phys. Usp. **16**, 459 (1974)].
[33]G. A. Askar'yan and B. A. Dolgoshein, cit. in Ref. 6, p. 553; Preprint No. 160, Lebedev Physics Institute, M., 1976; Pis'ma Zh. Eksp. Teor. Fiz. **25**, 232 (1977) [JETP Lett. **25**, (1977)].
[34]T. Bowen, as in Ref. 6, p. 523.
[35]G. A. Askar'yan, Atom. Energ. **3**, 152 (1957).
[36]V. D. Volovik and V. T. Lazurik-Él'tsufin, Fiz. Tverd. Tela (Leningrad) **15**, 2305 (1973) [Sov. Phys. Solid State **15**, 1538 (1974)].
[37]B. L. Beron and R. Hofstadter, Phys. Rev. Lett. **23**, 184 (1969); I. A. Borshkovskiĭ, V. D. Volovik, *et al.*, Pis'ma Zh. Eksp. Teor. Fiz. **13**, 546 (1971) [JETP Lett. **13**, 390 (1971)].
[38]V. D. Volovik and G. B. Khristiansen, as in Ref. 8b, Vol. 8, p. 3096.
[39]L. D. Landau and E. M. Lifshitz, Mekhanika sploshnykh sred (Fluid Mechanics), Nauka, M., 1968 (English transl. published by Pergamon Press, Oxford, 1975).

Translated by S. Chomet